MINISTRY OF EDUCATION AND RESEARCH
National University of Science and Technology POLITEHNICA Bucharest
Doctoral School of Industrial Engineering and Robotics

Bogdan-Ionuț CRISTEA

Doctoral Thesis Summary

RESEARCH ON ENHANCING PERFORMANCE OF FEED SYSTEMS FOR ULTRASONIC ASSISTED MICROELECTROEROSION

Doctoral Committee

President	**Prof. dr. ing.** Nicolae IONESCU	National University of Science and Technology POLITEHNICA Bucharest
Scientific adviser	**Prof. dr. ing.** Liviu Daniel GHICULESCU	
Referent	**Prof. dr. ing.** Oana DODUN-DES-PERRIERES	Technical University "Gheorghe Asachi" Iași
Referent	**Prof. dr. ing.** Aurel Mihail ȚIȚU	University "Lucian Blaga" Sibiu
Referent	**C.S.1 dr. ing.** Mihai MĂRGĂRITESCU	National Institude of Research and Development in Mechatronics and Measurement Technique Bucharest

~ 2024 ~

Keywords: *feed system, ultrasonic concentrator, ultrasonic assisted microelectroerosion*

Chapter 1. State of the Art in Electroerosion Development

Electroerosion (**E**lectric **D**ischarge **M**achining - EDM), the most used unconventional technology, belongs to the category of **thermal erosion** processes because it uses thermal energy to melt, vaporize and even boil the material of the processed workpiece [1].

1.1. Stages of the material removal mechanism

There are numerous models that explain the phenomenology of EDM, yet it remains insufficiently elucidated as the process unfolds geometrically on a micrometric or even nanometric scale, and temporally on a microsecond or less scale.

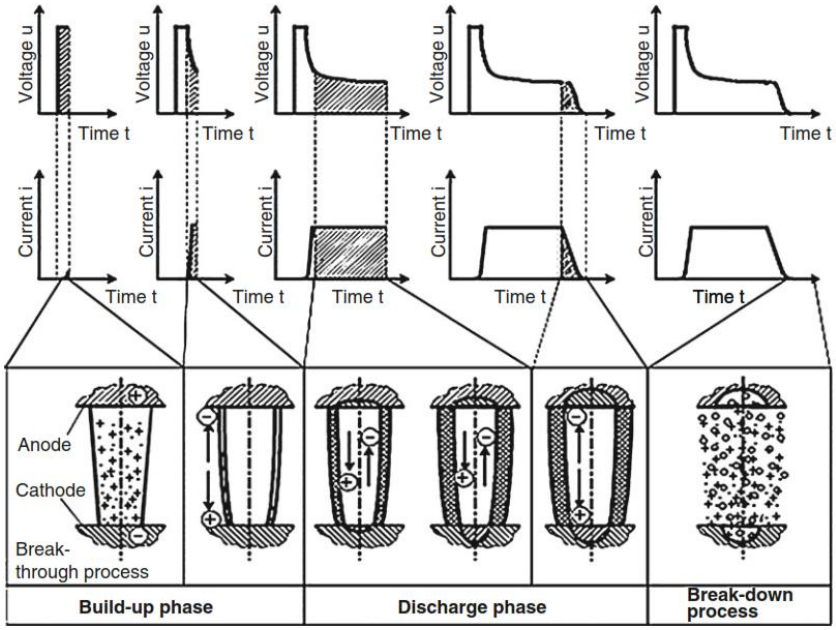

Figure 1.1 Principle of EDM [2]

In **Figure 1.1**, the stages of plasma channel formation during discharge and material removal are presented in correspondence with the variation of discharge voltage and current.

Within the EDM process, there are multiple types of discharges, depending on the time evolution of the discharge voltage (U_e) and discharge current (I_e), as depicted in **Figure 1.2**.

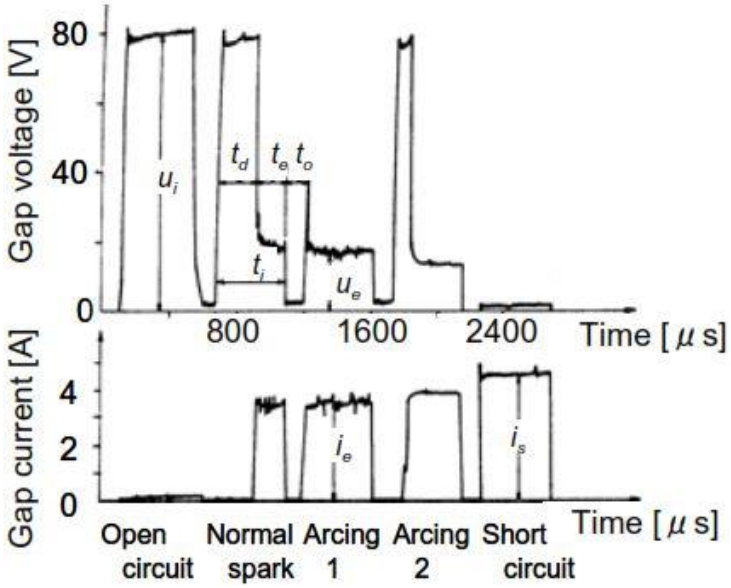

Figure 1.2 Various EDM discharges [6]

1.2. Gas bubble life duration and related phenomena

The plasma channel is formed during discharge between the surfaces of the tool and workpiece, whose temperature is approximately 10000 °C. This forms a gas bubble around the plasma channel.

In **Figure 1.3**, the evolution of the gas bubble is depicted, where it can be observed that its size is much larger than the plasma channel and the EDM spot.

a) Pre-ignition-Phase | b) Breakdown Phase | c) Phase after breakdown

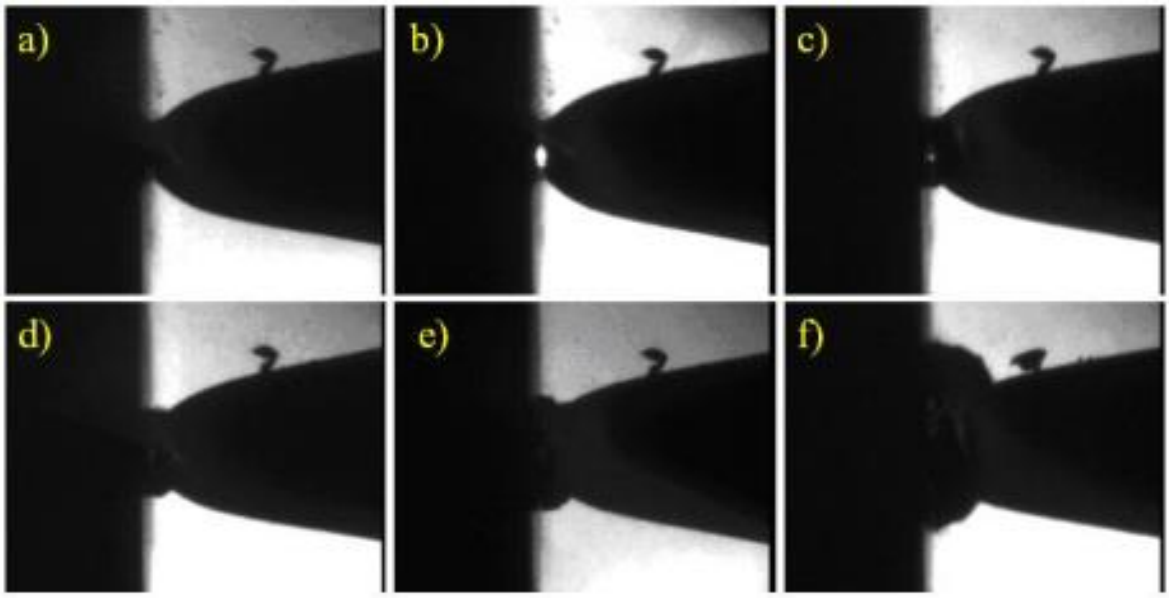

d) Evolution after 3 µs | e) Evolution after 6 µs | f) Evolution after 120 µs

Figure 1.3 Evolution of the gas bubble in EDM with the following parameters: I_{max} = *25 A*, t_i = *6 µs*, s_F = *15 µm*, hydrocarbon-based dielectric liquid [4]

In the classical electroerosion process, the gas bubble can persist long after the electrical discharge has ended. As a result, the molten discharge material solidifies before hydraulic forces can remove it, reducing the efficiency of the process [3**]**.

1.3. Electroerosion performance

Table 1.1 presents a comparison between conventional and non-conventional processes [1].

Table 1.1 Performance comparison of conventional and non-conventional processes [1]

Processes	**Maximum Productivity**	**Specific Productivity**	**Max. Precision**	**Minimum Roughness (Ra)**	**Tool consumption**
	[mm^3/min]	**[mm^3/(min/kW)]**	**[mm]**	**[µm]**	**-**
Cutting					
Roughing	10^5	10^4	0.01	6.3	Yes
Finishing	10^3	10^3	0.001	0.08	Yes
Superfinishing	1	10^2	0.00001	0.0001	Yes
Non-conventional					
Electroerosion	***10^3***	***10***	***0.0001***	***0.05***	***Yes***
Plasma	10^5	10^3	0.5	25	Yes
Laser	10	10	0.01	1.6	Nu
Electron Beam	10^2	10	0.01	1.6	Nu
Ultrasounds	10^2	10^2	0.005	0.1	Yes

Chapter 2. State of the Art of Microelectroerosion and Ultrasonic Assistance Development

Microelectroerosion (microEDM) is a variant of the EDM process, operating at micrometric scale (1 ÷ 999 μm), characterized by: very low energy level of discharge and a very narrow work gap, with negative consequences on process instability [2].

2.1. Differences between electroerosion and microelectroerosion

The microEDM process is similar to EDM, however, there are several differences, namely:

a) The most important difference is the size of the plasma channel. In EDM, the plasma channel is much smaller than the tool-electrode. In microEDM, the plasma channel is comparable in size to the tool-electrode [8] (**Figure 2.1**);

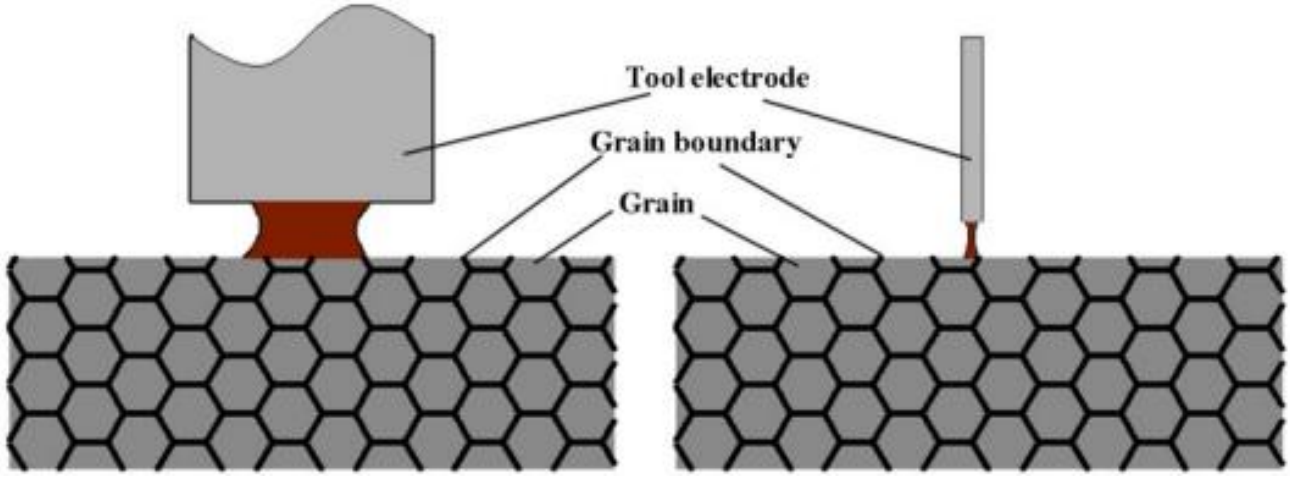

(a) macro EDM (b) micro EDM

Figure 2.1 Difference between plasma channel at macro EDM (a) and micro EDM (b) [10]

b) Small electrodes (< Ø30 μm) used in microEDM process cannot dissipate the heat emitted by the discharge due to their small volume. They also have a small mass, and at high discharge energies they can break. This enforces a maximum discharge energy limit. The difference between the discharge energies is visible in **Figure 2.2** indirectly, through crater size [8].

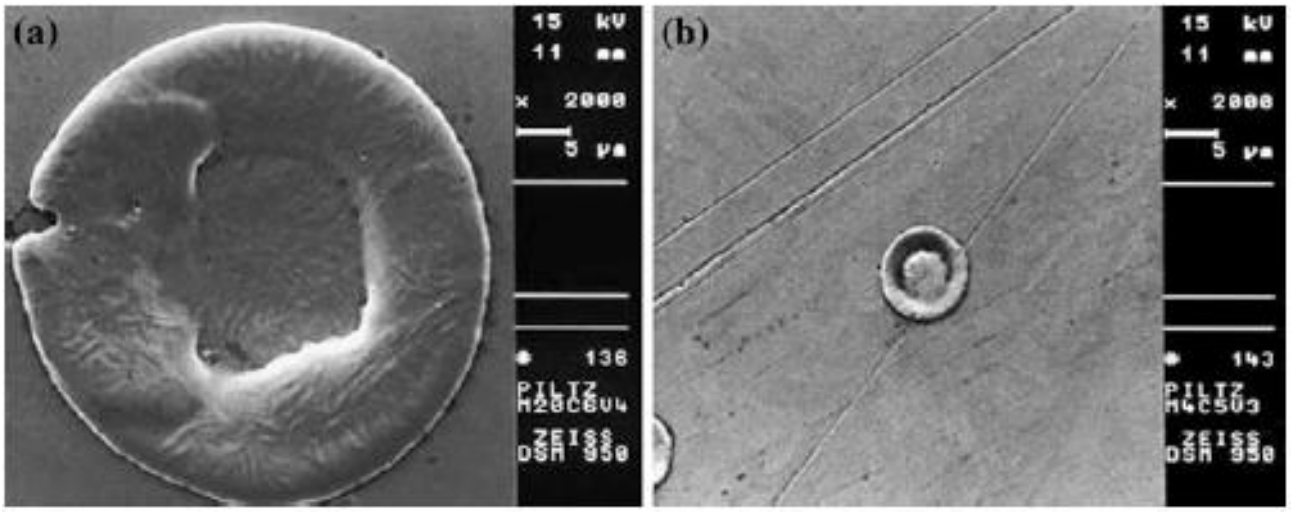

Figure 2.2 Comparison of crater size at **(a)** EDM (left) 20 μm and at **(b)** microEDM (right) 5 μm [8]

c) The flushing pressure acting on the tool-electrode is higher in microEDM than in EDM because the dielectric fluid needs to penetrate a much narrower work gap;

d) With each discharge, the wear of the tool-electrode is significantly higher in microEDM;

e) In microEDM, the maximum amount of energy must be limited to ensure the integrity of the tool-electrode. As a result, the amount of material removed per discharge is small. The craters in microEDM are much smaller than those in conventional EDM (**Figure 2.2** a) [8].

f) In macro EDM, the main goal is to ensure high productivity with acceptable precision and roughness. In microEDM, the primary objective is to achieve surfaces with low roughness and high precision. Therefore, there is also a limitation on the discharge energy.

The microEDM process occurs in **difficult conditions due to the very narrow work gap (ranging in size from 1 ÷ 5 μm),** which creates major difficulties in evacuating the removed material, leading to process instability and extremely low productivity.

2.2. Microelectroerosion performance

To better understand the characteristics of the microEDM process, Wong et al. [11] conducted an investigation into the differences in material removal mechanisms between EDM and microEDM. A capacitor-based generator generating a single discharge was used.

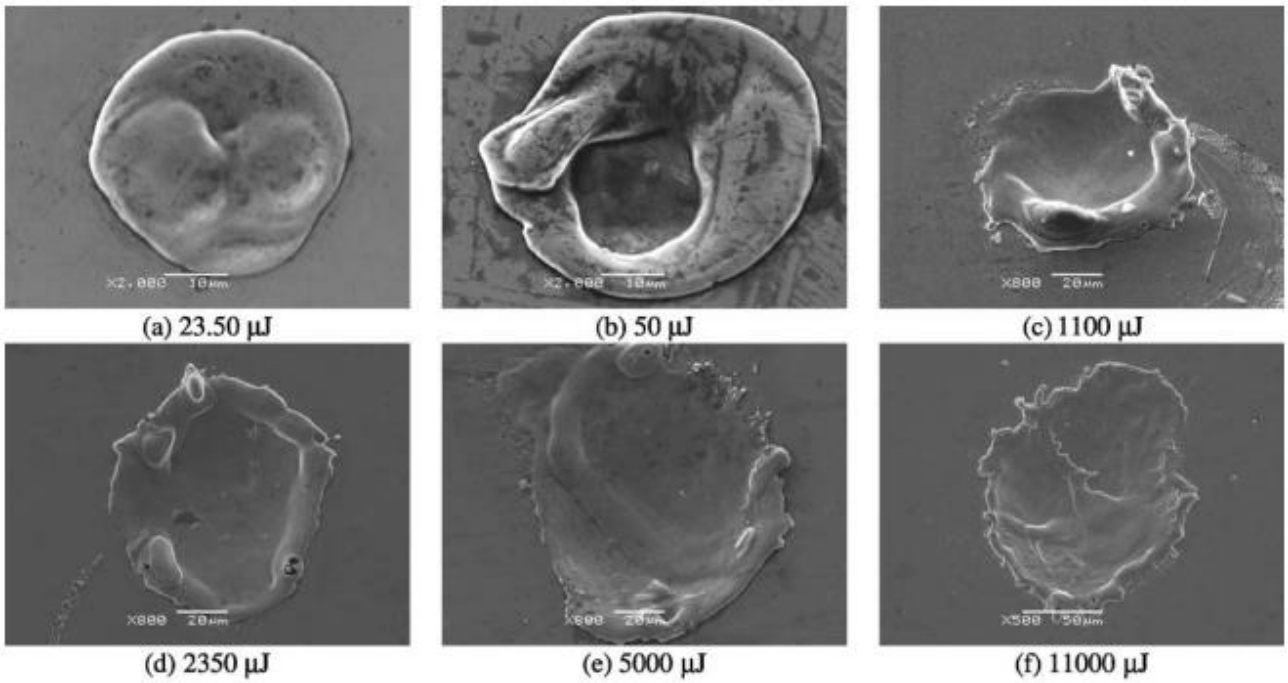

Figure 2.3 Micro-craters at a working gap of 2 μm for various discharge energies [11]

The following conclusions were reached (**Figure 2.3**) [11]:

1) The volume and diameter of micro-craters show less variation at low-energy discharges (< 50 μJ) compared to those at high energies;

2) The specific energy required for material removal is much lower at low discharge energy values (< 50 μJ) compared to higher discharge energies;

3) The efficiency of material removal at low discharge energies (< 50 μJ) is 7-8 times higher than at high discharge energies.

2.3. Limitations of microelectroerosion

An ideal EDM process delivers an identical amount of energy and achieves a consistent crater shape with each discharge (in the case of an isoenergetic EDM generator). The efficiency rate of microEDM is estimated to be between 30 and 50%, meaning that a portion of discharges is not optimal. Short-circuiting and sparking in the air negatively impact productivity, lead to wear on the tool-electrode, and result in deviations from the intended shape [9].

In **Figure 2.4**, the requirements for a stable microelectroerosion process (A) and the disadvantages, along with a series of solutions (B), are presented.

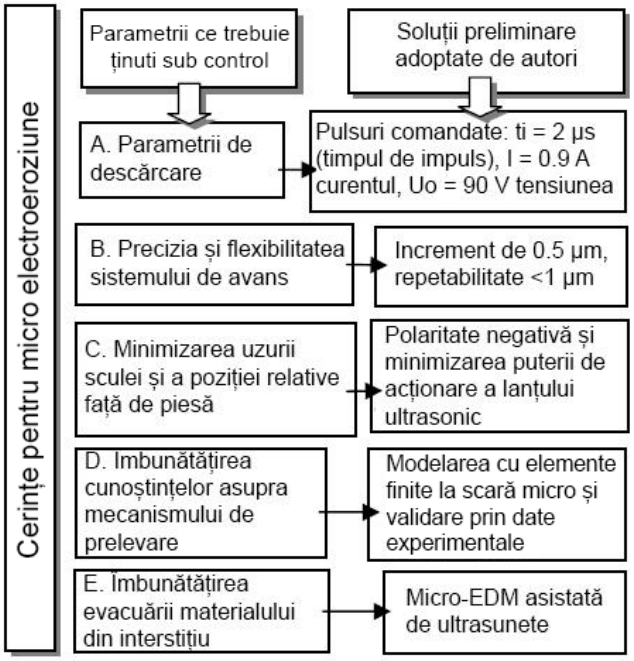

A. Requirements for microEDM [12]

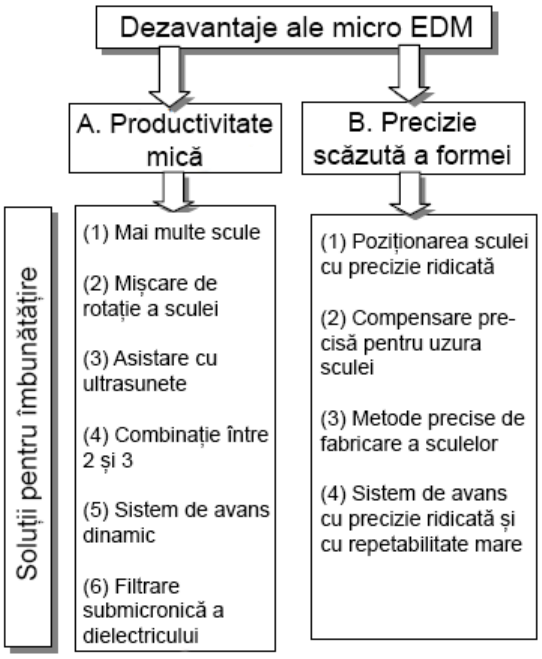

B. Disadvantages of microEDM [13]

Figure 2.4 Requirements and disadvantages of microEDM

2.4. Ultrasonic assistance of microelectroerosion

In the current trend of modern technology, the demand for precise and small-sized components made from extremely hard materials is continuously growing, therefore conventional machining processes struggle to meet these requirements. Therefore, hybrid systems have been designed: ultrasonic assisted electroerosion machining (EDM+US) and ultrasonic assisted microelectroerosion machining (microEDM+US) - which have successfully increased process stability, productivity, and surface quality.

Ultrasonic (US) refers to high-frequency waves that exceed the upper limit of human hearing perception. Generally, a frequency is considered to be in the ultrasonic range if it exceeds 20 kHz, extending up to 1 GHz [7].

Pulse duration – when processing EDM+US there is an overlap of ultrasonic oscillations over the duration of discharges (pulse time).

Any ultrasonic machining setup includes an ultrasonic generator, which converts the industrial frequency of 50 Hz from the alternating current of the power grid into ultrasonic frequency (> 20 kHz). This frequency is then applied to the transducer within the ultrasonic chain.

The ultrasonic chain (**Figure 2.5**), is responsible for generating ultrasonic vibrations and locating them, at maximum amplitude, at the tip of the tool.

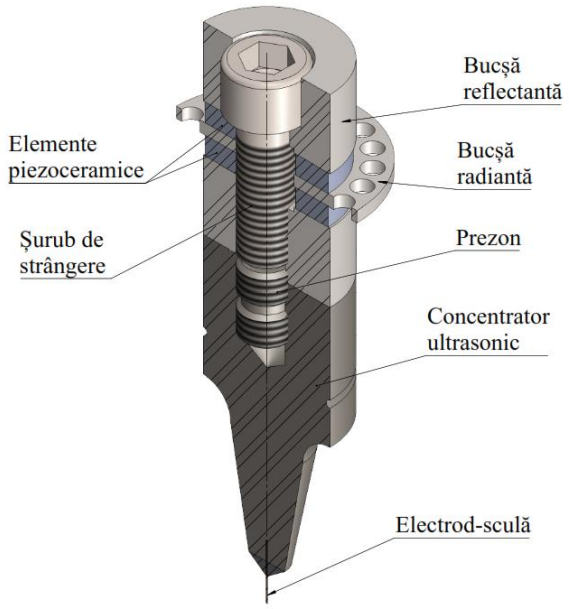

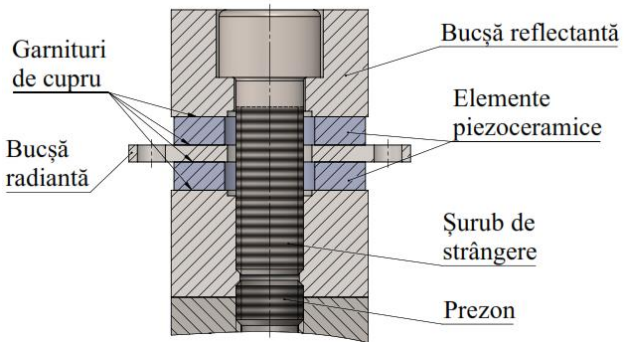

Detail – Ultrasonic transducer and the assembly with the ultrasonic concentrator

Figure 2.5 Structure of an ultrasonic chain used in ultrasound assisted microelectroerosion

2.5. Phenomena in ultrasonic assisted electroerosion process

In general, EDM and microEDM superfinishing processes take place in a work gap on the order of µm, leading to frequent occurrence of negative phenomena such as short-circuiting or continuous arcing. These issues are caused by the difficult evacuation of particles removed during the process and have a significant impact on productivity (V_w), relative volumetric wear (θ), and the quality of the obtained surface.

Ultrasonic assistance, with the ultrasonic frequency vibration of the tool-electrodes, aims to eliminate the specific instability of the microEDM process [12] [13] and enhance its precision, surface quality, and productivity performance.

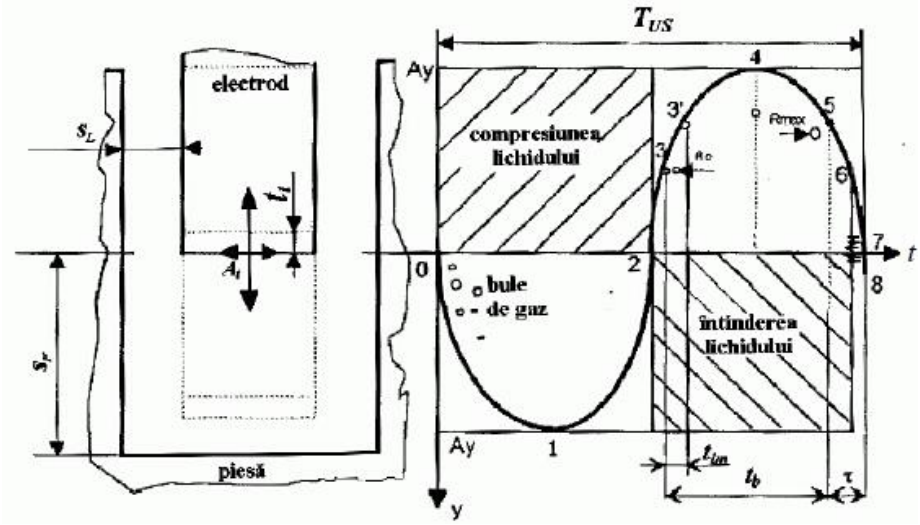

Figure 2.6 Specific phenomena in EDM+US [15]

The removal mechanism of EDM+US has two main components:

I. Thermal phenomena (EDM)

Material is removed through melting, vaporization, and even boiling, following the superheating model proposed by Van Dijck and Snoeys, confirmed by experimental data [33] due to the formation of a plasma channel between the tool-electrode and the workpiece, as well as the formation of a gas bubble due to the vaporization of material and dielectric fluid..

II. Ultrasonically induced cavitation phenomena in the frontal work gap

Ultrasonic oscillation of the tool-electrode in electroerosive machining is subject to specific constraints related to the amplitude (A) used. In a fixed reference system tOy (attached to the EDM installation, as per **Figure 2.6**), an essential condition must be met to avoid short-circuiting phenomena during the EDM process – the stability condition [15].

This assumes that the amplitude *A* is less than the work gap.

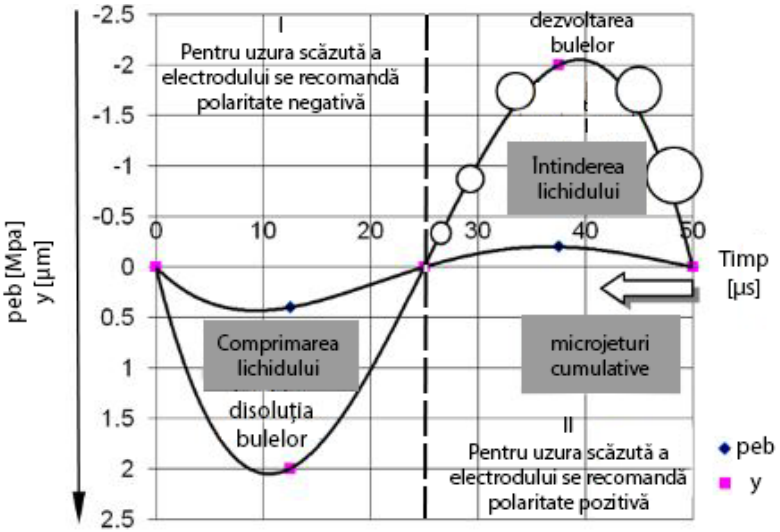

Figure 2.7 Ultrasonically induced cavitation phenomena in EDM+US at a frequency of 20 kHz [5]

The modeling of the EDM process assisted by the longitudinal ultrasonic vibration of the tool-electrode highlights specific phenomena related to the values of elongation y, as illustrated in **Figure 2.6**. The oscillation period (T_{US}) is divided into two half-periods (**Figure 2.6** and **Figure 2.7**):

I) In the first semiperiod the dielectric fluid compression occurs

The reduction of the frontal work gap s_F in the first half-period promotes the occurrence of discharges between the electrodes.

II) In the second semiperiod (25 – 50 µs) at f_{us} = 20 kHz, the dielectric fluid undergoes stretching

The pressure of the dielectric in the working gap becomes negative and the volume of gas bubbles resulting from an electrical discharge, which has previously occurred, increases to a value corresponding to a high hydraulic pressure at the end of a period of oscillation. At this time, cumulative microjets are formed as a result of the implosion of gas bubbles in the work gap [15]. This phase is characterized by pressures of the order of 100 MPa, much higher than those of the usual EDM, producing low values of relative wear due to the large volume of material removed by ultrasonic assistance.

During **cumulative microjet phase**, maximum pressures of the order of hundreds of MPa are produced – with orientation parallel to the processed surface, which allows roughness reduction (*Ra*), by removing surface microgeometry peaks that have low shear strength [15].

The development of the plasma channel is stopped by very high pressures during the cumulative microjet phase.

2.6. Ultrasonic assisted microelectroerosion performance

Increasing productivity, achieving cavities with a high aspect ratio (the ratio between depth and transverse size), improving process stability, and reducing negative phenomena (short-circuit,

continuous arc) can all be achieved through ultrasound-assisted machining. The main cause of these limitations in microEDM is the inefficient flushing of the micrometer-scale work gap.

Increasing the frequency of vibrations leads to a decrease in processing time (**Figure 2.8**), since particle evacuation becomes more efficient by increasing the number of phases of cumulative microjets produced per unit of time.

The effect of vibration is small for amplitudes of 0.3 μm and 0.5 μm (**Figure 2.9**). For amplitudes of 1 μm and 1.5 μm, a significant reduction in processing time is observed. The results can be extrapolated fundamentally, even in the domain of ultrasonic vibrations.

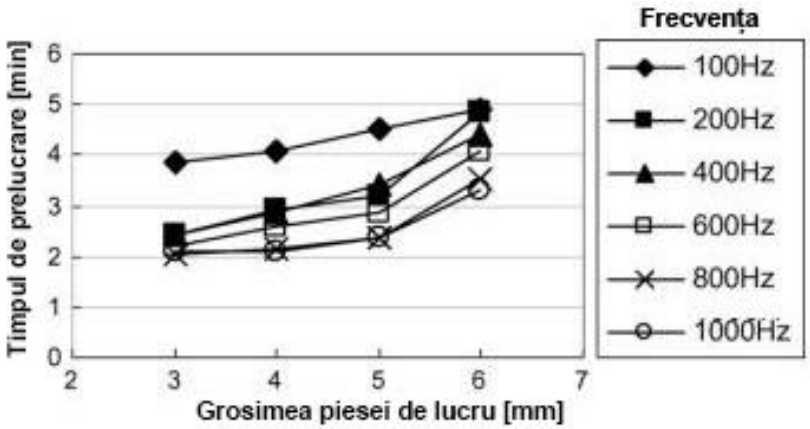

Figure 2.8 Effects of vibration frequency on processing time with $A = 1\ \mu m$ [17]

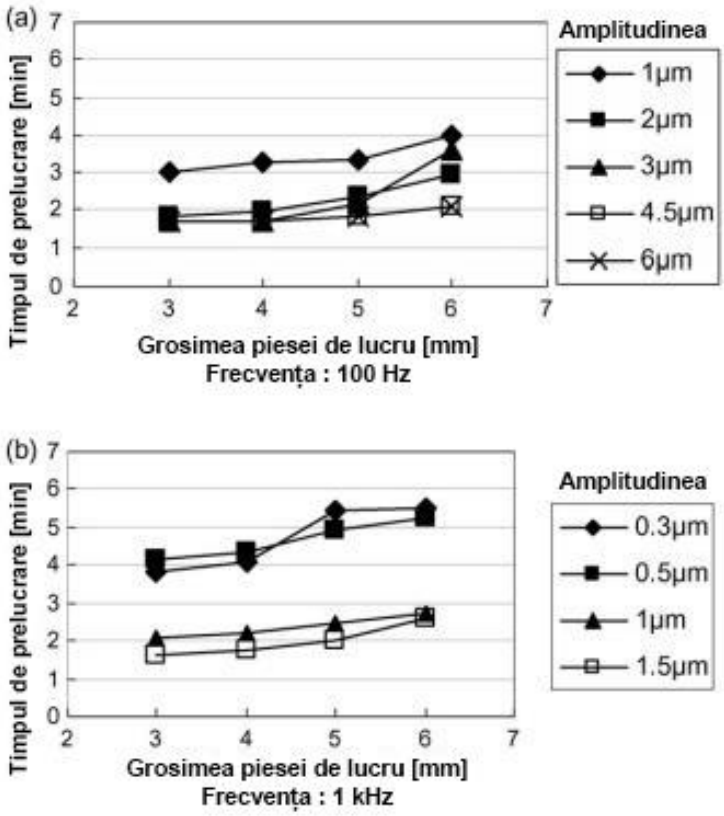

Figure 2.9 Effects of vibration amplitude on processing time [17]

Chapter 3. State of the Art of Feed Systems for Electroerosion Development

An electroerosion machining installation consists of three main assemblies: the machine tool itself, the electroerosive pulse generator and power supply (conventional circuit), and the dielectric fluid unit. These sub-assemblies are interdependent; the malfunction of one of them leads to the inability to operate the EDM installation [18].

3.1. Servo control system

The servo system makes analog decisions based on the discharge voltage in the working interstice or, alternatively, based on the initiation delay time [18]. The dielectric fluid is an insulator until the breakdown voltage is applied, after which it becomes an electrical conductor. The point at which the dielectric fluid becomes an electrical conductor is called the ionization point. The transition from insulator to conductor leads to a decrease in voltage between the tool-electrode and the workpiece, from the breakdown voltage (U_a) to the discharge voltage (U_e), as shown in **Figure 3.1**.

Once the discharge occurs, the discharge voltage varies within a wide range; therefore, it is recommended that the reference point of the voltage (used by the servo system) be within the variation range so that the process is as stable as possible [18].

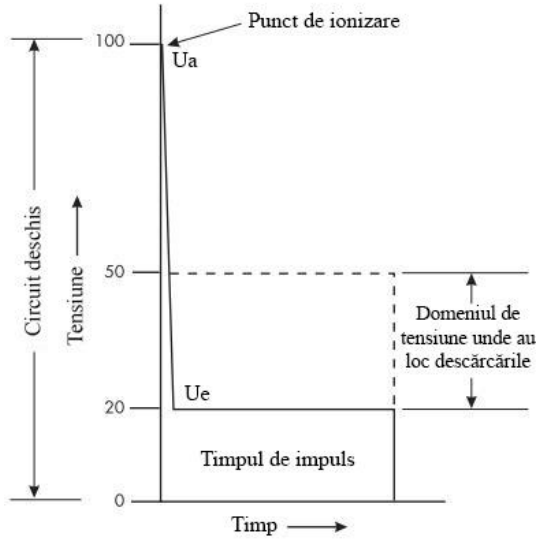

Figure 3.1 Voltage range during discharge [18]

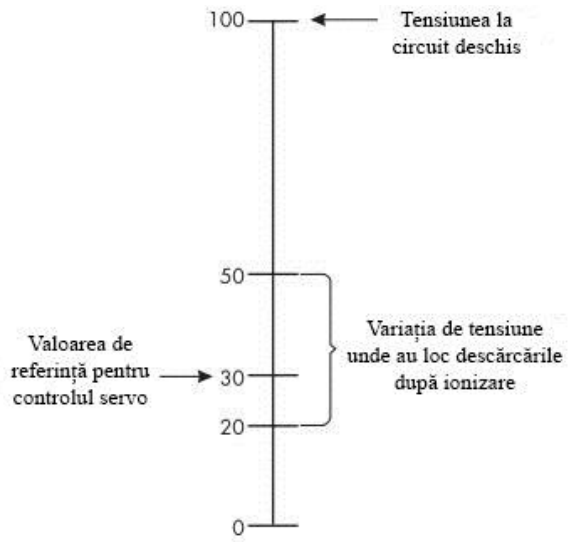

Figure 3.2 Reference value in the discharge voltage range [18]

A reference value for the servo system control will be chosen from the discharge voltage range. The reference voltage is compared with the voltage in the work gap (according to **Figure 3.2**). The difference between these two values is used to advance, retract, or maintain the electrode-tool.

3.2. Positioning and accuracy of feed systems

The response time between the command to advance/retract the tool-electrode and its execution must be less than 10 ms under finishing processing conditions, which involve a frontal work gap of less than 10 μm [14].

The requirements for the implementation of feed systems for micro-machining are:

1. Reaction speed of the feed system;

2. High geometric and positioning accuracy;

3. Optimization of the micro-electroerosion process to achieve minimal wear and high quality of the machined surface..

The fundamental element from which the optimization of EDM technologies starts is the adequate dynamics of the electroerosive feed system. This is expressed by the response time of the system (Δt) according to the relationship [14]:

$$\Delta t = \Delta t_{MPP} + \Delta t_j + \Delta t_f + \Delta t_e \; [s] \qquad \textbf{(3.1)}$$

where: Δt_{MPP} – delay produced by the drive motor of the feed system [s]; Δt_j – delay produced by clearances in the system [s]; Δt_f – delay due to overcoming friction forces [s]; Δt_e – delay caused by the elastic elements of the feed system [s].

The work gap must be large enough to allow the evacuation of particles and small enough to allow as many discharges as possible during the machining process.

3.3. Control systems

The purpose of any electronic control system is to measure, monitor, and control a specific process. One way to monitor a process is by comparing output data with input data to reduce the difference between the obtained result and the programmed result.

Advantage: Precision, facilitates automation, allows adaptation to disturbances;
Disadvantage: Difficult to design, high acquisition and maintenance costs.

For the control of the electroerosion process, there are various control systems [15], namely:

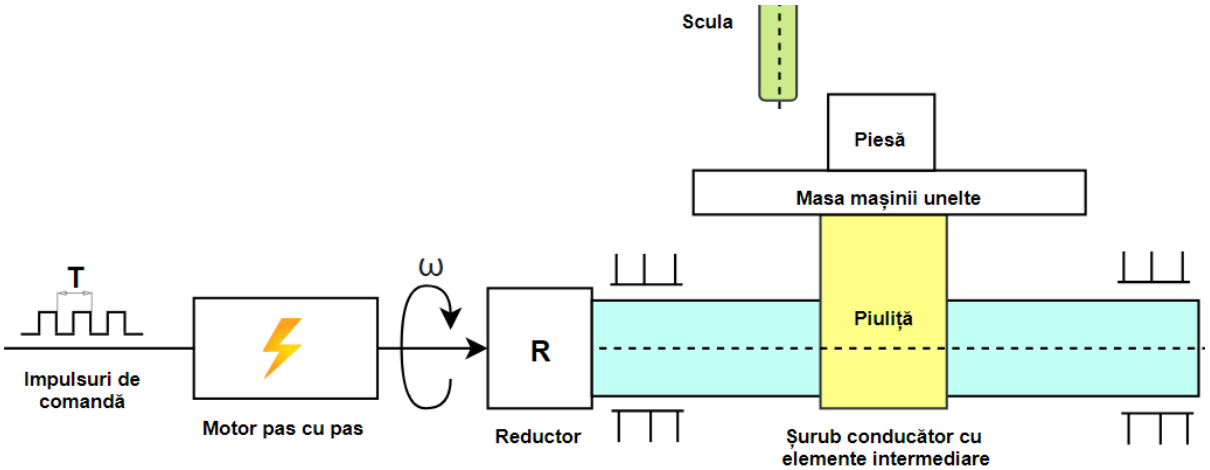

Figure 3.3 Structure of an open-loop control system, after [15]

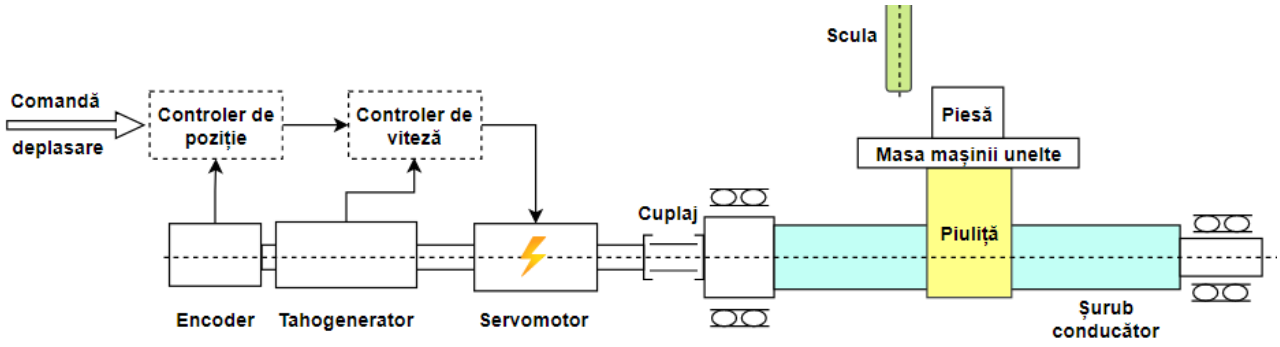

Figure 3.4 Structure of a semi-closed-loop control system, after [15]

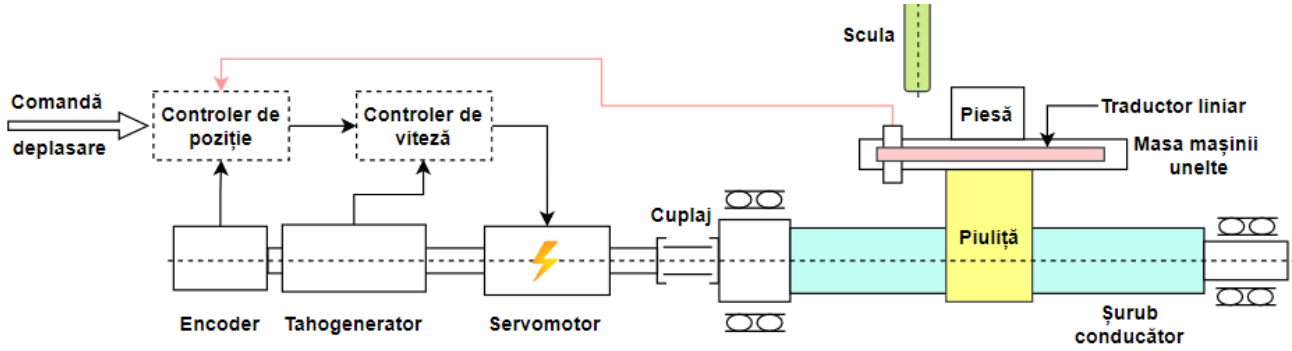

Figure 3.5 Structure of a closed-loop control system, after [15]

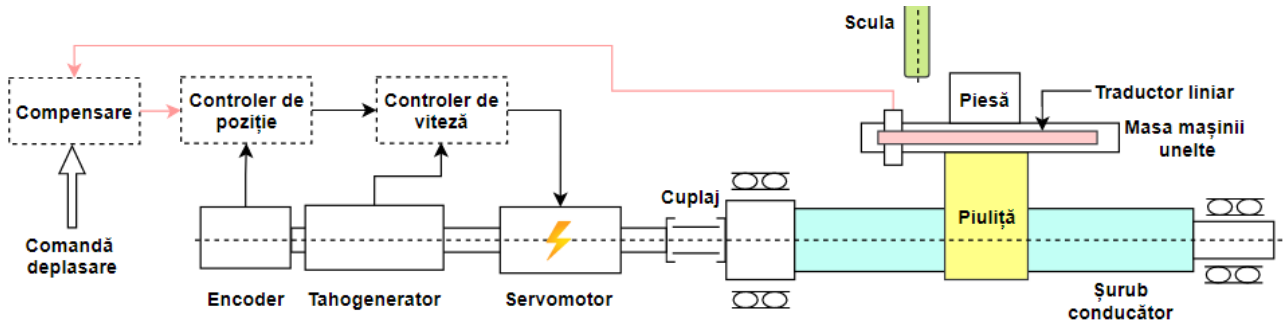

Figure 3.6 Structure of a hybrid control system, after [15]

1. Open-loop control system. It uses a stepper motor (MPP), which is controlled by a control unit through current pulses (see **Figure 3.3**). Each pulse determines the angular displacement with a certain increment. Precision is influenced by the stepper motor, coupling, ball screw, and other intermediate elements.

2. Semi-closed-loop control system. The semi-closed loop is a widely used solution due to reduced costs and satisfactory precision. The angular position of the ball screw is determined by the encoder mounted on the motor shaft, and the linear displacement of the table/workpiece depends on the precision of the lead screw step. Displacement corrections are made after identifying lead screw step errors (see. **Figure 3.4**).

3. Closed-loop control system. Involves the use of a linear transducer to measure the linear displacement of the table, which is mounted on the frame. As a result, the precision of the ball screw no longer has an impact on positioning accuracy, as the system feedback is obtained after the lead screw has completed the movement (see **Figure 3.5**).

4. Hybrid control system. Combines two types of loops: a semi-closed loop that uses an encoder to detect position, and a closed loop that uses a linear transducer (see **Figure 3.6**).

Chapter 4. Conclusions on the State of the Art of Ultrasonic Assisted Microelectroerosion and Feed Systems

After analyzing and researching the state of the art of electroerosion, ultrasonic assisted electroerosion, and the development of feed systems, several significant conclusions have emerged, on whose basis **part II Contributions to the Realization of Feed Systems for Ultrasonic Assisted Microelectroerosion** is constructed. The conclusions are:

1. Process parameters of EDM and microEDM:

- The values of electrical and non-electrical parameters have a significant impact on the technological performance of the EDM process. Discharge voltage, discharge current, pulse duration, and the capacitor capacity of relaxation generators are adjusted by adaptive systems to optimize productivity, surface roughness, and tool electrode wear;
- The pause time in the EDM process is crucial for process stability and efficient evacuation of removed material. An optimal ratio between pulse time and pause time is necessary to prevent short-circuits and maintain productivity;
- The electrical resistance of the electrode-tool – workpiece material couple, as well as the local conductivity of the dielectric fluid in the working gap, influences discharge energies, directly impacting the efficiency of the EDM process;
- Flushing techniques and flushing pressure affect the stability of the microEDM process, which occurs in challenging conditions determined by the narrow work gap with values of 1 – 5 μm. Proper combination of these methods leads to significant improvements in the output technological parameters of the machining process.

2. Ultrasonic assisted microelectroerosion (microEDM+US):

- The microEDM process has limitations regarding the size of the electrode-tool and the work gap, as well as discharge energies, resulting in lower productivity compared to EDM;
- Ultrasonic assistance brings significant benefits to the technological performance of microEDM by adding an additional material removal mechanism generated by ultrasonically induced cavitation phenomena in the work gap;
- The frequency and amplitude of ultrasonic vibrations can be adjusted to improve material evacuation and the quality of the processed surface. These parameters, along with those of the microEDM processing regime, can be optimized to achieve the best results.

3. Feed systems:

- The response time of electromechanical feed systems is in the order of milliseconds, highlighting the importance of reducing it;
- Optimal response time is essential for process accuracy, surface quality, productivity, and tool wear. A reduced response time ensures efficient processing;
- Implementing a feed system with a low response time can maximize the benefits of the microEDM+US process by improving the efficiency of material removal from the work gap.

Chapter 5. Objectives, Research Directions and Methodology addressed in the Doctoral Thesis

5.1. Synthesis of critical aspects regarding the state of the art of ultrasonic assisted microelectroerosion and advance systems development

1. The current trend of ultra-miniaturization in the field of processing technologies, aiming to reduce the dimensions of generated surfaces, aligns with the challenges imposed by Industry 4.0. This trend includes the technology of ultrasonic-assisted micro-electroerosion. The increase in data transmission speed, information storage capacity, and the speed of operation of technological system elements is closely connected to the concentration of energies in very small spaces for processing materials and components. This is a characteristic feature of unconventional technologies, also referred to as concentrated energy technologies, as seen in the case of microEDM.

2. Conventional micro-electroerosion has the ability to process surfaces of very small dimensions at lower costs compared to other similar technologies in the micro domain, using various technological systems, where the feed system - positioning the electrode-tool in relation to the machined surface - plays a crucial role in the material removal process. The micro domain is defined within the range of 1 - 999 μm according to the CIRP (College International pour la Recherche en Productique / The International Academy for Production Engineering).

3. The limitations of micro-electroerosion are related to the instability of the process determined by the size of the machining gap (generally 1-5 μm) in connection with very low discharge energy, in the range of 10^{-9} – 10^{-5} J, volume of removed material: 0.05 – 500 μm^3 and the inefficient evacuation of particles from the machining gap – inefficient flushing. Under these conditions, frequent short-circuit phenomena occur between the electrode-tool and the machined surface, accompanied by a decrease in productivity due to repeated retraction and approach strokes of the electrode-tool performed by the feed system, as well as a reduction in the quality (deterioration) of the machined surface.

4. The specificity of the micro-electroerosion process under the conditions of longitudinal vibration of the electrode-tool with ultrasonic frequency, in this case, approximately 20 kHz, and more commonly, 40 kHz, involves the modification of the frontal work gap with this frequency through the elongation of the electrode-tool - amplitude in the order of micrometers - positioned at the end of the ultrasonic chain at a point of maximum amplitude (ventru), adding additional instability.

5. In addition to this potential additional instability in microEDM+US, ultrasonically induced cavitation in the work gap improves the material removal process, provided that the feed system in microEDM+US does not cause a short circuit between the surfaces of the electrode-tool and the workpiece. Through the variation of hydrostatic pressure in the work gap - pumping of the dielectric fluid, thus improved flushing and evacuation, additional removal of both solid and liquid material occurs due to the implosion of gas bubbles in the work gap at the end of each liquid dielectric stretching semiperiod.

6. The ultrasonic assistance in microEDM can lead to a several-fold increase in productivity, improved quality of the machined surface, and a reduction in relative volumetric wear. This justifies the research efforts to develop a suitable feed system for microEDM+US.

7. Under microEDM+US processing conditions, the feed system must meet additional and enhanced requirements compared to the feed system of conventional microEDM:

- The electrode-tool must move with very small incremental values (i) to prevent short-circuit phenomena between the electrode-tool and the machined frontal surface, especially critical

in the case of a frontal work gap in the range of 1 - 5 μm, care se modifică cu valorile elongației electrodului-sculă, which changes with the values of the elongation of the electrode-tool, at the micrometer level, and that depends on the amplification provided by the ultrasonic concentrator, at each ultrasonic period, $T_{us}=25\mu s$, if the frequency is $f_{us} = 40\ kHz$;

- Excellent dynamics in executing retract and approach commands, evaluated through the response time (Δt) of the advance or retract command, at most 10 ms;

- Clamping the ultrasonic chain in a nodal plane, ensuring that the ultrasonic vibrations of the ultrasonic chain integrating the tool do not propagate inside the feed system.

7. The construction of the feed system in microEDM+US must include elements to reduce the response time (Δt) by decreasing the inertia of the feed system drive motor; reducing elastic deformation when applying the torque; reducing screw-nut friction; reducing clearance between the threads of the screw and nut.

8. The performance of feed systems for ultrasonically assisted microelectroerosion can be evaluated using four parameters: positioning accuracy, resolution (increment size), dynamics (response time of feed and retract commands), and the level of vibrations within the feed system.

A critical analysis of relevant aspects from the current state of affairs formed the systemic basis for the formulation of the thesis objectives.

5.2. Research directions and methodology of the doctoral thesis

The major research directions (*Di*) to be pursued within the doctoral thesis will be as follows, with possible specifications of sub-directions that will prove important for enhancing the performance of feed systems for ultrasonic-assisted microelectroerosion and the connected material processing process:

(D1) Conceptual design and application of methods to enhance the quality of a feed system for ultrasonic-assisted microelectroerosion;

(D2) Detailed design of a feed system for ultrasonic-assisted microelectroerosion;

(D3) Detailed design of a clamping device for the ultrasonic chain, which integrates the tool electrode, for a feed system for ultrasonic-assisted microelectroerosion;

(D4) Modeling and simulation of the operation of a feed system for ultrasonic-assisted microelectroerosion;

(D5) Implementation of a feed system for ultrasonic-assisted microelectroerosion;

(D6) Implementation of an ultrasonic chain integrating the tool electrode for ultrasonic-assisted microelectroerosion;

(D7) Testing of the feed system for ultrasonic-assisted microelectroerosion;

(D8) Testing of an ultrasonic chain integrating the tool electrode for ultrasonic-assisted microelectroerosion;

5.3. Objectives of the doctoral thesis

Following the critical analysis of the current state of technological systems for microEDM and microEDM+US, particularly focusing on suitable feed systems for microEDM+US, the following have been established: **a main objective (*Op*)** and several **specific objectives (*Osi*)**. To facilitate their achievement, these objectives have been formulated in a logical and gradual sequence, as presented below:

Op: The main objective of the doctoral thesis is to design, implement, and test an *efficient* feed system for the process of ultrasonic-assisted microelectroerosion.

The transition aimed to progress from the conceptual stage, reaching the level of technological maturity (Technology Readiness Level) TRL 2, to the stage of a functional model under laboratory conditions, specifically TRL 4 [34] [35] [36].

Several **specific objectives** (subordinate) were established, detailed from the main objective, as follows:

Os1: Conceptual design of a feed system for ultrasonic-assisted microelectroerosion – TRL 2;

Os2: Application of methods to improve the quality of the feed system for ultrasonic-assisted microelectroerosion;

Os3: Detailed design of an efficient feed system for ultrasonic-assisted microelectroerosion;

Os4: Detailed design of an ultrasonic chain that integrates the electrode-tool;

Os5: Detailed design of a clamping device for the ultrasonic chain;

Os6: Modeling and simulation of the operation of a feed system for ultrasonic-assisted microelectroerosion;

Os7: Modeling and simulation of the operation of an ultrasonic chain that integrates the electrode-tool;

Os8: Physical realization of an efficient feed system for ultrasonic-assisted microelectroerosion;

Os9: Physical realization of an ultrasonic chain that integrates the electrode-tool;

Os10: Testing a feed system for ultrasonic-assisted microelectroerosion in laboratory conditions – TRL 4;

Os11: Testing an ultrasonic chain that integrates the electrode-tool in laboratory conditions – TRL 4;

5.4. Research methodology

The research and development methodology designed to achieve the main objective and secondary objectives includes the following stages:

E1. Critical analysis of the state of the art of technological systems for microEDM and microEDM+US, as well as suitable feed systems for microEDM+US;

E2. Conceptual design of an efficient feed system suitable for microEDM+US - Technology Readiness Level **2**, **TRL 2**;

E3. Improvement of a designed feed system by applying recognized methods for quality enhancement;

E4. Design of a clamping system for the ultrasonic chain integrating the tool, considering the nodal point position (minimum amplitude of ultrasonic wave oscillation) to minimize vibrations within the feed system;

E5. Modeling and simulation of a feed system with essential parameters - eigenfrequency and deformations under certain critical operating conditions;

E6. Modeling and simulation of a US chain integrating the tool, achieving resonance conditions, maximizing amplification, and determining the nodal point;

E7. Technological process design and implementation of an efficient feed system, as well as the US chain integrating the tool and clamping system;

E8. Testing a feed system and the US chain integrating the tool in laboratory conditions - Technology Readiness Level **4**, **TRL 4**.

Chapter 6. Conceptual Design of the Feed System for Ultrasonic Assisted Microelectroerosion

6.1. Formulation of the functions of the feed system

The feed system is a mechanism that: moves the tool (workpiece) to perform machining operations, positions (orients) the tool/workpiece for technological operations along a linear/circular (rotational) axis, enhances machining precision either through new concepts related to the machine tool (mechanical hardware) or by real-time correction of the tool position relative to the coordinate system (software), and enables the implementation of innovative machining procedures.

A feed system for microEDM+US has the **general function** of positioning the tool electrode. This general function ensures the attainment of an optimal frontal work gap for the production of EDM discharges between the tool electrode and the workpiece, considering the variation of this gap due to the ultrasonic vibrations of the tool electrode.

The functions of the feed system are summarized in **Table 6.1**.

Table 6.1 General function and main function of the feed system for microEDM+US

General Function (FG) - Positioning the tool electrode for the generation of discharges in microEDM+US conditions	
Nr.	**Main function**
Fp1	Performing advance/retract motions
Fp2	Analog measurement and continuous indication of position
Fp3	Executing movements with velocity and acceleration profiles
Fp4	Transforming rotational motion into translational motion
Fp5	Perpendicularity of the feed system to the machine table
Fp6	Executing movements with minimal response time and minimal demands on the feed system
Fp7	Minimizing the transmission of vibrations in the feed system
Fp8	Adjusting the inclination of the feed system for inclined holes
Fp9	Operating the feed system outside resonance
Fp 10	Achieving submicron linear incremental displacement

6.2. Identification of solutions

The following **Table 6.2** outlines solutions to be adopted for each function. Adopted solutions are highlighted in gray.

Table 6.2 Solutions for the main functions of the feed system

Main function	Structure / Block	Solutions			
		A	**B**	**C**	**D**
Fp1. Performing advance/retract motions	Motion execution	Roller screw	Pneumatic cylinder	Hydraulic cylinder	…
Fp2. Analog measurement and continuous indication of position	Monitoring system Execution system	Monitoring system provided by the actuation element (driver)	Monitoring system tailored to the application (custom-created)	-	…
Fp3. Executing movements with velocity and acceleration profiles					
Fp6. Executing movements with minimal response time and minimal demands on the feed system					
Fp4. Transforming rotational motion into translational motion	Auxiliary elements	Guiding column and roller	-	-	…
Fp5. Perpendicularity of the feed system to the machine table	Auxiliary elements	Clamping plate	-	-	…
Fp7. Minimizing the transmission of vibrations in the feed system	Auxiliary elements	Small contact surface	Isolation through plastic/rubber parts	-	…
Fp10. Achieving submicron linear incremental displacement	Motion execution	Electric motor	Hydraulic motor	Ultrasonic motor	…
Fp2. Analog measurement and continuous indication of position (process monitoring)	Process monitoring system	Discharge voltage monitoring system	Discharge types monitoring system	-	…
Fp8. Adjusting the inclination of the feed system for inclined holes	Auxiliary elements of the execution system	Rotary plate, screws, nuts and washers			
Fp9. Operating the feed system outside resonance	Ultrasonic chain connection element	Prisms	Clamping between tips	-	…

6.3. Selection of solution variants

6.3.1. Screw-nut mechanism

Funcționally, the screw-driven transmissions are listed in **Table 6.3**, and graphically represented in **Figure 6.1** [20].

Table 6.3 Functional variants of transmissions

Variant	Motion element / motion	Driven element / motion
a	Screw / rotation	Nut / translation
b	Nut / translation	Screw / rotation
c	Screw / translation	Nut / rotation
d	Nut / rotation	Screw / translation

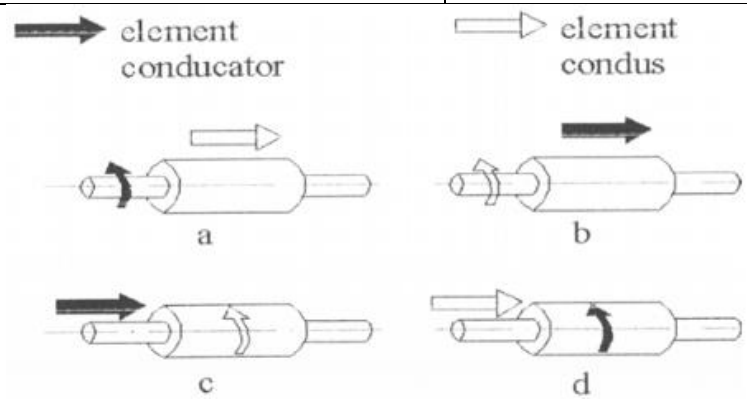

Figure 6.1 Functional variants for screw-nut transmissions [20]

The screw-nut mechanism with rollers is applicable to feed systems. The load is transmitted from the nut to the shaft through the cylindrical surfaces of all the involved rollers. The diameter of the contact surface is significantly increased with the number of contact points.

From a **functional** standpoint, the driving element is the screw, performing a rotational movement (**Table 6.3**), and from a **structural** standpoint, a screw-nut system with rollers is chosen.

6.3.2. Coupling

For the feed system, a flexible coupling is chosen to compensate for the non-coaxiality between the motor shaft and the screw shaft, with the risk of adding to the response time of the feed system. This choice is justified by the fact that, although it introduces a delay (due to flexibility), this can be compensated for or reduced to a value that does not significantly affect the precision of the system.

6.3.3. Drive motor

The types of electric motors most commonly used in the industry are servo motors and stepper motors. Neither of them is a universal solution for all types of applications. The choice of motor type depends primarily on speed, acceleration, and cost.

A. Stepper motor

The stepper motor (MPP) is an electromechanical device that converts a sequence of digital pulses into linear or rotational motion proportional to the number of pulses. The rotor moves in discrete and successive angular steps, each of equal size, referred to as motor steps. To operate correctly, the number of steps executed by the motor must correspond to the number of command pulses applied to it.

B. Servo motor

A category of motors called micro stepper motors, with mounting dimensions LxW of 60 x 60 mm, has been identified. From this category, **From this** table, the five-phase stepper motor **CRK564PMBP** is selected, which has the smallest rotor inertia to minimize residual motion after executing commands – the larger the residual motion, the lower the positioning accuracy.

Table 6.4 [21] is extracted, presenting several models of stepper motors. From this table, the five-phase stepper motor **CRK564PMBP** is selected, which has the smallest rotor inertia to minimize residual motion after executing commands – the larger the residual motion, the lower the positioning accuracy.

Table 6.4 Stepper motor characteristics [21]

Model	Single Shaft	**CRK564PMAP**	**CRK566PMAP**	**CRK569PMAP**
	Double Shaft	**CRK564PMBP**	**CRK566PMBP**	**CRK569PMBP**
Characteristic	**Unit of measure**			
Maximum Holding Torque	N*m	0.78	1.3	2.3
Rotor Inertia	$J/Kg*m^2$	$320*10^{-7}$	$500*10^{-7}$	$1100*10^{-7}$
Basic Step Angle	°	0.36		
Excitation Mode	-	Microstep		

6.4. Detailed application of Quality Function Deployment method

***Q**uality **F**unction **D**eployment* (QFD) is a structured system that facilitates the identification of customer requirements and expectations and translates them into technical language as an organizational response to these requirements. The purpose of this system is to interpret and integrate the "*voice of the customer*" into the quality characteristics of products, processes, and services so that customer needs and expectations can be met – the technical response or the voice of the company.

The result is presented in **Figure 6.2**.

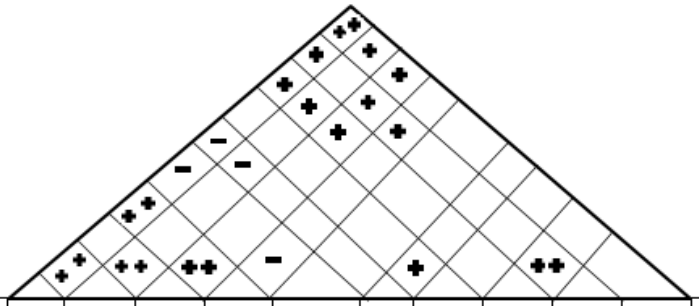

Direcția de îmbunătățire			x	x	▼	x	x	▲	x	▼	x	▼	Evaluarea concurenței după cerințele clienților			
Cerințele clienților	**Importanța**	**Importanța [%]**	Execuția deplasărilor de avans/retragere	Măsurarea analogică și indicarea continuă a poziției	Execuția deplasărilor cu timp de răspuns minim și solicitări minime ale sistemului de avans	Execuția deplasărilor cu profil adecvat de viteză și accelerație	Transformarea mișcării de rotație în mișcare de translație	Perpendicularitatea sistemului de avans pe masa mașinii	Reglarea înclinării sistemului de avans	Minimizarea transmiterii vibrațiilor în sistem	Funcționarea sistemului de avans în afara rezonanței	Deplasarea cu increment liniar submicronic	**1**	**2**	**3**	**4**
Precizia de prelucrare	84	**27.5**	●	●	●	●	●	●	●	○	●	●	5	5	5	5
Calitatea ridicată a suprafeței prelucrate	70	**22.9**	●	●	●	●	○	○	□	●	●	●	5	4	4	4
Productivitate ridicată	66	**21.6**	●	●	●	●	○	○	○	○	●	●	4	4	4	4
Fiabilitate ridicată	54	17.6	○	●	○	●	○	○	○	●	○	●	4	4	3	2
Compactitate ridicată	32	10.5	□	□	□	□	●	○	●	○	○	□	4	4	2	2
Impact global			710	816	710	816	527	465	482	543	731	816				
Impact global [%]			11	**12**	11	**12**	8	7	7	8	**11**	**12**				
Evaluarea tehnică a concurenței	**1**		5	5	4	4	5	5	5	4	5	5	✚ impact pozitiv ✚✚ impact puternic pozitiv ● corelare puternică (9) ○ corelare medie (3) □ corelare slabă (1)			
	2		5	5	4	4	5	5	5	4	5	5				
	3		5	4	4	4	5	5	1	2	4	4				
	4		5	4	3	4	5	5	1	1	4	4				
Obiective tehnice			Divizarea pasului prin intermediul driver-ului	Utilizarea unui encoder	Validarea timpului de răspuns minim	Adoptarea unui profil de viteză și accelerație sub forma unei curbe S	Utilizarea unei role de contact cu posibilitatea reglării poziției în raport cu coloana de ghidare	Plăci de prindere și suporți	Placă de prindere prevăzută cu canale circulare	Conectarea lanțului ultrasonic în planul nodal al concentratorului pe o suprafață redusă	Simularea intrării în rezonanță	Utilizarea preciziei în selectarea elementelor componente ale sistemului de avans				

Figure 6.2 QFD Matrix

6.5. Detailed application of Analysis of failure modes and their effects method

FMEA (**F**ailure **M**ode and **E**ffects **A**nalysis) is a systematic method for identifying and preventing product issues before they occur.

This analytical method aims to prevent defects, improve product or process safety, and ultimately enhance customer satisfaction..

This proves extremely effective when applied in the early stages of development, before the product is manufactured. However, in the case of complex products, such as the feed system for microelectroerosion assisted by ultrasonics, although necessary, the FMEA method can become challenging to apply. Therefore, it is often recommended to simultaneously use other complementary methods for a more comprehensive approach [22] [23].

Table 6.5 FMEA for the feed system

Failure mode and effects analysis												Action results				
Nr. crt.	**Component**	**Defect**	**Defect effect**	**Severity**	**Cause of defect**	**Occurrence**	**Detection and control measures**	**Detection**	**RPN**	**Recommended action**	**Responsibility / Completion time**	**Action taken**	**Severity**	**Occurrence**	**Detection**	**RPN**
1	Motor	Executes fewer steps than commanded	Low positioning accuracy	7	Wrong selection of MPP	3	Functional simulation	6	126	Change MPP	Design Manager / 1 day	Verification of the angular increment of the MPP	7	1	1	7
		Executes the commanded steps with delay	Low positioning accuracy	7	Wrong selection of MPP	4	Functional simulation	6	168	Change MPP	Design Manager / 1 day	Verification of the electronic command path	7	1	1	7
		Doesn't receive commands	Cannot be used	8	Incorrect connections	3	Functional simulation	2	48	Change MPP	Design Manager / 1 day	Verification of the electronic control circuit	8	1	1	8
		Excessive heating of the MPP	Cannot be used within optimal parameters	6	Usage outside the predicted parameters	4	Functional simulation	5	120	Change MPP	Design Manager / 1 day	Verification of the operating modes of the MPP	6	2	3	36
		Bearings failure	Low positioning accuracy	7	Lifespan exceedance	3	Functional simulation	9	189	Change MPP	Design Manager / 1 day	Verification of the prescribed operating hours	7	2	2	28
2	Driver	Incorrect pitch division	Low positioning accuracy	7	Low resolution	3	Functional simulation	5	105	Change driver	Design Manager / 1 day	Selection of the driver imposed by MPP	7	1	1	7
3	Screw-nut	Imperfect contact between threads	Low positioning accuracy	7	Design error	4	Functional simulation	5	140	Check calculations	Design Manager / 2 days	Check profile of screw and nut	7	2	2	28
		Clearance between threads	Low positioning accuracy	7	Design error	4	Functional simulation	5	140	Check calculations	Design Manager / 2 days	Check the tolerances for the screw and nut profile	7	2	2	28
		Inadequate axial pitch	Low positioning accuracy	7	Design error	4	Functional simulation	5	140	Check calculations	Design Manager / 2 days	Verify the calculation of the pitch for screw and nut	7	2	2	28

Failure mode and effects analysis												Action results				
Nr. crt.	**Component**	**Defect**	**Defect effect**	**Severity**	**Cause of defect**	**Occurrence**	**Detection and control measures**	**Detection**	**RPN**	**Recommended action**	**Responsibility / Completion time**	**Action taken**	**Severity**	**Occurrence**	**Detection**	**RPN**
4	Coupling	Inability to connect the motor shaft to the lead screw shaft	Cannot be used	10	Incorrect choice of the coupling	3	Functional simulation	2	60	Verification of the technical drawing of the screw-nut and the coupling documentation	Design Manager / 2 days	Comparison of the diameter of the motor shaft and the lead screw with the coupling's connecting diameter	10	2	1	20
5	Encoder	Faulty detection of movements	Inaccuracy in movement commands	7	Resolution outside of the range of the MPP	3	Functional simulation	5	105	Verification of motor and encoder documentation	Design Manager / 2 days	Selection of the encoder based on the resolution of the stepper motor	7	1	1	7
6	Guiding column	The roller does not make contact with the guide column	Impairs accuracy	7	Wrong adjustment	4	Functional simulation	5	140	Check adjustment	Design Manager / 2 days	Establish the position of the contact roller and the displacement interval	7	1	2	14
		The contact pressure is excessive	Inaccuracy in movement commands	7	Design error	4	Functional simulation	5	140	Check adjustment	Design Manager / 2 days	Establish the position of the contact roller and the displacement interval	7	1	2	14
7	Ultrasonic chain	Introduces vibrations within the feed system	Impairs accuracy	7	Wrong identification of the nodal channel	3	Functional simulation	5	105	Verification of the technical drawing and functional simulation	Design Manager / 2 days	Verification of the oscillation amplitude on the contact surface of the ultrasonic concentrator	7	2	2	28

6.5.1. Calculation of the Economic Efficiency Number

A supplementary hierarchy of actions/measures is undertaken on the causes of defects based on the Economic Efficiency Number **NEE** [24**]**.

NEE is calculated with the following relation:

$$NEE = RIA * CIA * IRN \quad \textbf{(6.1)}$$

where:

RIA – Rapidness of Action Implementation, on a scale from 1 to 10 (very fast 10, very slow 1);

CIA – Cost of Action Implementation, on a scale from 1 to 10 (very cheap 10, very expensive 1);

IRN – Impact on Risk Number Reduction (RPN), estimates how quickly the risk number has been reduced, on a scale from 1 to 10 (very fast 10, very slow 1);

The following table outlines all the proposed actions:

Table 6.6. Economic efficiency number NEE

Nr. Crt.	Remedy actions for RPN	RIA	CIA	IRN	NEE
1	Verification of the prescribed operating hours	9	9	10	810
2	Check the tolerances for the screw and nut profile	8	9	9	648
3	Comparison of the diameter of the motor shaft and the lead screw with the coupling's connecting diameter	9	8	9	648
4	Selection of the driver imposed by MPP	8	8	10	640
5	Verification of the angular increment of the MPP	7	8	10	560
6	Check profile of screw and nut	7	8	9	504
7	Verify the calculation of the pitch for screw and nut	7	8	9	504
8	Selection of the encoder based on the resolution of the stepper motor	7	7	10	490
9	Verification of the electronic command path	6	7	10	420
10	Establish the position of the contact roller and the displacement interval	6	8	8	384
11	Verification of the electronic control circuit	5	6	10	300
12	Verification of the operating modes of the MPP	4	6	10	240
13	Verification of the oscillation amplitude on the contact surface of the ultrasonic concentrator	3	3	9	81

Finally, measures are adopted with priority in decreasing order of the NEE factor.

Chapter 7. Detailed Design of the Feed System for Ultrasonic Assisted Microelectroerosion

The structure of the feed system that resulted from the conceptual design process is presented in **Figure 7.1**:

1. The screw-nut mechanism – transforms rotational motion into translational motion, with precision being influenced by the type of mechanism;

2. Actuation elements – responsible for driving and controlling the feed system;

3. The ultrasonic chain – leads to the improvement of stability and performance in the micro-electroerosion process;

4. Connecting elements – establish the connection between components and ensure the transmission of movements.

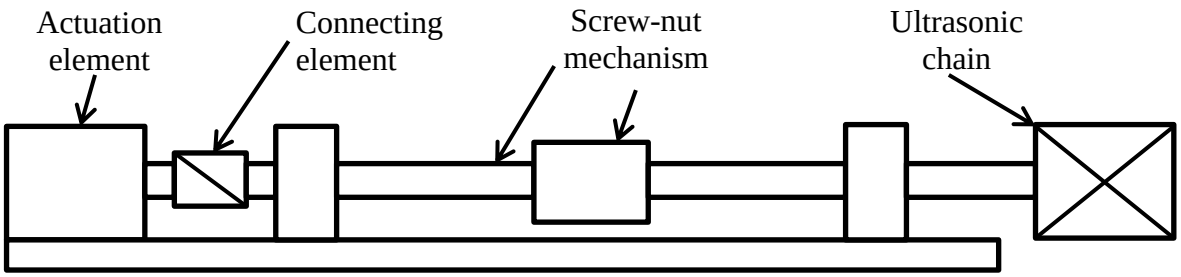

Figure 7.1 Feed system structure for microEDM+US

From the previous chapter, the electric stepper motor was chosen as the actuation element, the screw-nut mechanism with rollers as the executing element, and elastic couplings as connecting elements.

7.1. Screw-nut mechanism

Screw-nut mechanisms are used to transform rotational motion into translational motion, either for transmitting large forces (force transmissions) or solely for cinematic purposes (motion transmissions) [19].

7.1.1. Sizing of key areas

In this stage, bearings are selected to reduce friction between the lead screw and fixed support 1, and between the nut and fixed support 2, thereby reducing the response time of the advancement system in the microEDM+US processing. The advancement system has two support points: one allowing the rotation of the lead screw, mounted on the first support, and another mounted on the second support, enabling the translation of the nut (**Figure 7.2**).

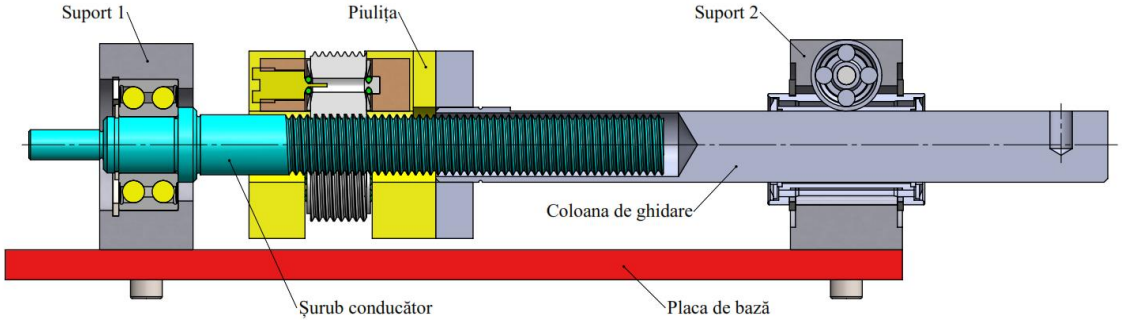

Figure 7.2 The feed system and the two fixed supports fixe of the lead screw

1) Bearing for the lead screw

After selecting the bearing type, [26] s used to choose the specific bearing based on the required permissible static load capacity ($C_{0a\ req}$). The chosen bearing is 3202 A-2RS1TN9/MT33 [27], whose characteristics are presented in **Table 7.1**:

Table 7.1 Data for bearing 3202 A-2RS1TN9/MT33 [26]

Bore diameter d [mm]	**Outside diameter D [mm]**	**Width B [mm]**	**Basic dynamic load rating C_a [N]**	**Basic static load rating C_{0a} [N]**
15	35	15.9	11200	6800

As seen in the table, $C_{0a\ req} = 1466\ N < C_{0a} = 6800\ N$, thus the bearing satisfies the necessary conditions for being used in the screw-nut mechanism.

The tolerance for the shaft diameter ***Ø15 j5*** $\left(^{+0.005}_{-0.003}\right)$ is chosen from the "*seat tolerances for standard conditions*", recommended for applications where the load direction is undetermined, and the inner ring undergoes rotational motion. The tolerance for the housing ***Ø35 H7*** $\left(^{+0.025}_{0}\right)$ is selected, recommended for various loads where the outer ring is stationary [27].

2) Linear bearing for the nut

The nut performs a translational motion, so a linear bearing/bushing with balls is required to guide the guide column that undergoes translational motion with minimal friction. A preselection is made for a linear bearing LME-20-UU-OP [28] and the static load is calculated. This type of bearing features a free zone corresponding to a flat surface on the guide column, which will be used to restrain the rotational motion of the nut, allowing it to perform only translational motion. It is recommended to have a diameter of ***Ø32 P7*** $\left(^{-0.017}_{-0.042}\right)$ for the housing, forming a press fit with the linear bearing. The linear bearing data is presented in **Table 7.2**:

Table 7.2 Data for the linear bearing LME-20-UU-OP [28]

Bore diameter d [mm]	**Bore diameter tolerance [mm]**	**Outside diameter D [mm]**	**Outside diameter tolerance [mm]**	**Width B [mm]**	**Basic dynamic load rating C_a [N]**	**Basic static load rating C_{0a} [N]**
20	$20^{+0.009}_{-0.001}$	32	$32^{0}_{-0.011}$	45	863	1370

In the inner sleeve of the linear bearing, there are four channels with recirculating balls, each channel having 10 balls in contact with the guide column, highlighted in **Figure 7.3**.

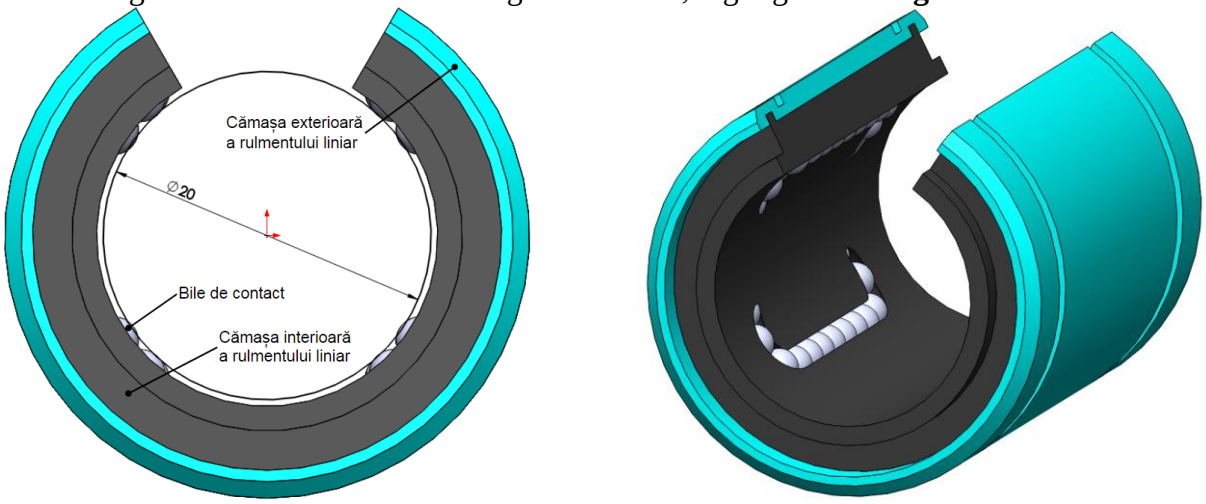

Figure 7.3 3D model of the linear bearing LME-20-UU-OP, according to the data from [28]

The static load capacity (C_{0n}) is calculated with the following formula [28]:

$$C_{0n} = S_s * q * F_a\ [N] \qquad \textbf{(7.1)}$$

where: S_s – contact surface of a ball [mm^2]; d_c – diameter of the guide column [mm]; q – number of balls in the linear bearing [balls]; $q = 40$ *balls*; F_a – axial load; $F_a = 10$ *N*.

In order to calculate the contact surface, the difference between the diameter of the guide column ($d_c = 20^{+0.020}_{+0.012}\ mm$) and the inner diameter of the bearing ($d = 20^{+0.009}_{-0.001}\ mm$) is calculated for the four relevant cases highlighted in **Table 7.3**.

The difference between diameters (d_{dif}) is calculated using the formula:

$$d_{dif} = d\ - d_c\ [mm] \qquad \textbf{(7.2)}$$

Subsequently, d_{dif} is used in the 3D model (**Figure 7.4**) to determine the contact area (S_s) between the guide column and the linear bearing ball using the "*Measure*" command in Solidworks.

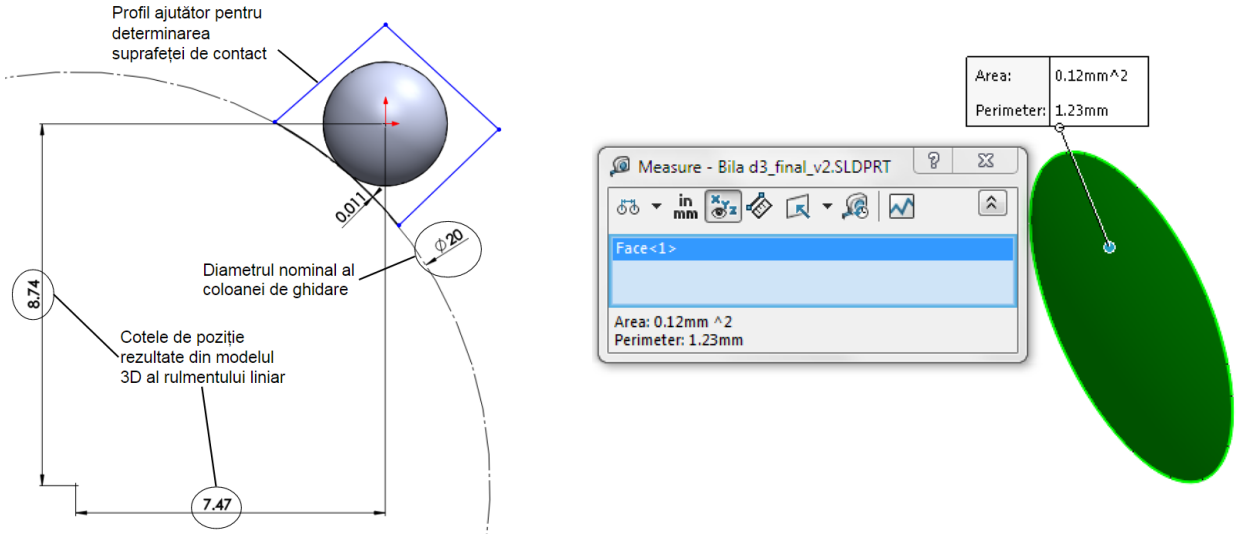

a) Geometric model b) Contact surface S_s

Figure 7.4 Determining the contact area of the ball with the guide column shaft for case I

The static load capacity (C_{0n}) for the four possible cases are presented in **Table 7.3**.

Table 7.3 Possible cases

Case I		**Case II**	
d_c = 20.02 mm	d = 20.009 mm	d_c = 20.02 mm	d = 19.999 mm
$d_{dif1} = 20.02\ -\ 20.009\ =\ 0.011\ mm$		$d_{dif2} = 20.02\ -\ 19.999\ =\ 0.021\ mm$	
S_{s1} = 0.12 mm^2		S_{s2} = 0.21 mm^2	
$C_{0n1} = 0.12 * 40 * 10\ =\ 48\ N$		$C_{0n1} = 0.21 * 40 * 10\ =\ 84\ N$	
Case III		**Case IV**	
d_c = 20.012 mm	d = 20.009 mm	d_c = 20.012 mm	d = 19.999 mm
$d_{dif3} = 20.012\ -\ 20.009\ =\ 0.003\ mm$		$d_{dif4} = 20.012\ -19.999\ =\ 0.013\ mm$	
S_{s3} = 0.05 mm^2		S_{s4} = 0.14 mm^2	
$C_{0n3} = 0.05 * 40 * 10\ =\ 20\ N$		$C_{0n4} = 0.14 * 40 * 10\ =\ 56\ N$	

The linear bearing has an allowable static load (the maximum load a bearing can withstand before permanent damage occurs; indicates a static load applied in a constant direction) C_{0a} = *1370 N*, which is higher than the calculated values in the table, therefore, the bearing is suitable for use within the screw-nut mechanism.

After this initial pre-sizing, based on the selection of the two bearings, the design of the actual lead screw follows.

7.2. Leading screw design

The lead screw is structurally designed, taking into account the sizing of the key areas highlighted in the previous stage. The lead screw is presented in **Figure 7.5**:

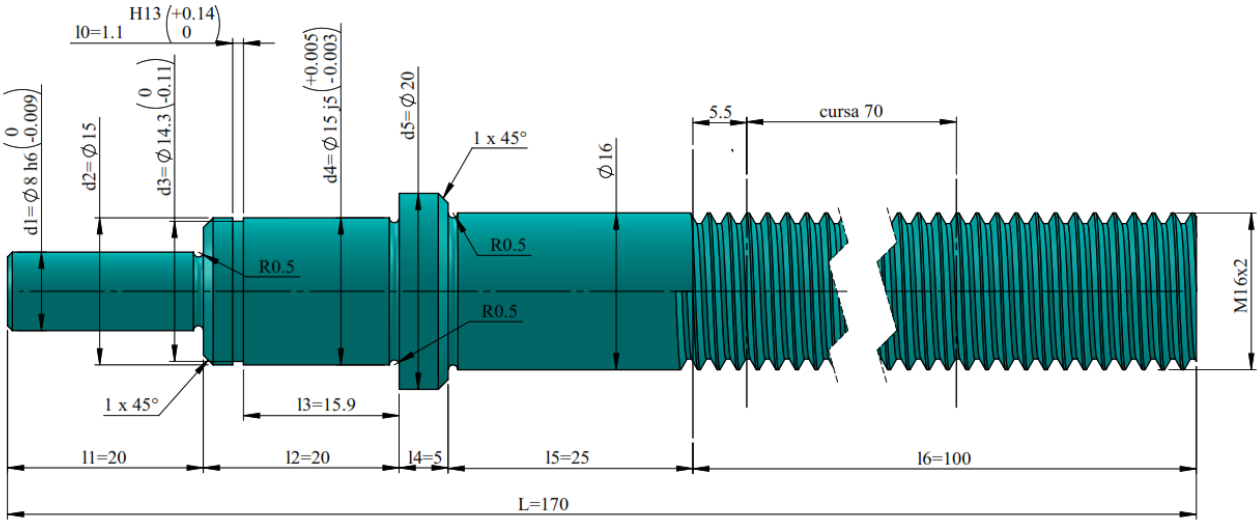

Figure 7.5 Lead screw

Starting from the left part (**Figure 7.5**), with a diameter of d_1 = ***Ø8 h6*** $\left(^{0}_{-0.009}\right)$, necessary for connecting the motor shaft to the lead screw through a coupling. The coupling gripping length is l_1 = ***20 mm***. Next is d_2 = ***Ø15***, which features a location with a channel length of l_0 = ***1.1 H13*** $\left(^{+0.14}_{0}\right)$, and d_3= ***14.3*** $\left(^{0}_{-0.11}\right)$, according to DIN 471 for a retaining ring, used to secure the bearing presented in **Figure 7.6**. The clearances between surfaces with different diameters have the shape of semicircular channels with R0.5 mm.

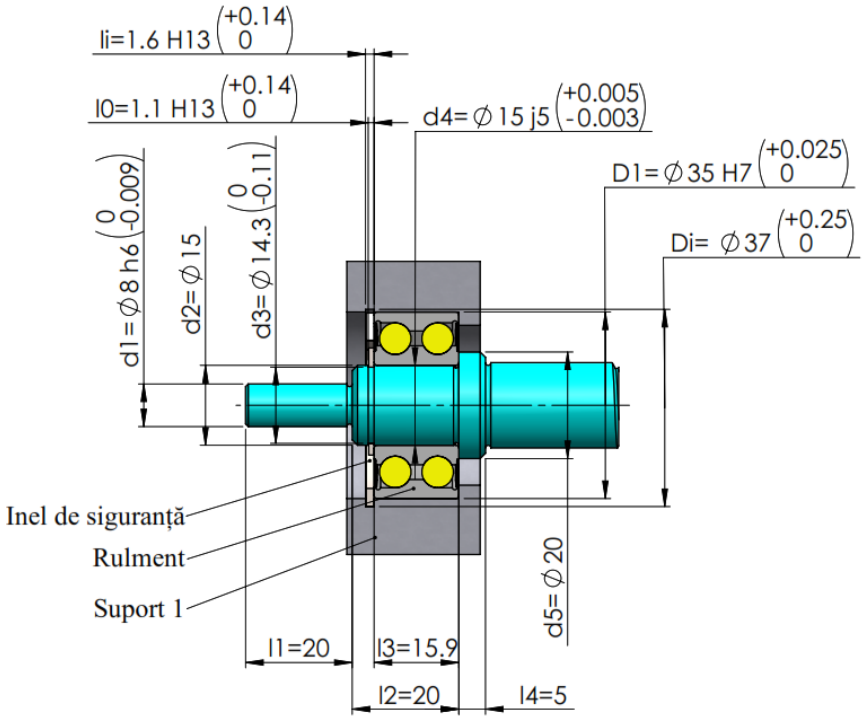

Figure 7.6 Bearing assembly detail

Over the length l_3 = ***15.9*** the double-row angular contact bearing 3202 A-2RS1TN9/MT33 [27] is mounted, and the shaft diameter is recommended to be d_4 = ***Ø15 j5*** $\left(^{+0.005}_{-0.003}\right)$ to secure the

inner ring of the bearing to the shaft. The inner diameter of the support, where the bearing is mounted, is recommended to be $\boldsymbol{D_1 = Ø35\ H7}\ \binom{+0.025}{0}$. The support has a housing for a retaining ring to secure the outer ring of the bearing, with dimensions recommended by DIN 472, $\boldsymbol{D_i = Ø37}\ \binom{+0.25}{0}$ and $\boldsymbol{l_i = 1.6\ H13}\ \binom{+0.14}{0}$.

Next is the shoulder to which the bearing is fixed, that is recommended to be larger than Ø16 [27], a condition met by $\boldsymbol{d_5 = Ø20}$. The length $\boldsymbol{l_4 = 5}$ is chosen constructively. Next is the region defined by $\boldsymbol{l_5}$ and the diameter ***Ø16***, whose length is recommended by SKF [25] to be **greater than 12 mm**. The value $\boldsymbol{l_5}$, (see **Figure 7.5**) meets this condition. On the right side, there is an **M16x2** thread with a length of $\boldsymbol{l_6 = 100}$ and a constructive chosen working stroke of **70 mm**, highlighted in **Figure 7.5**. The 70 mm portion is the range in which the rollers can move. The unspecified chamfers dimension is 1x45˚.

7.3. Roller and nut design

In this stage, the constructive design of the roller and nut is carried out. The lead screw comes into contact with a certain number of rollers. Thus, the design starts with a roller, knowing that the lead screw has a diameter of M16 and a pitch of 2 mm. **Figure 7.7** presents the designed roller with a length of 15 mm.

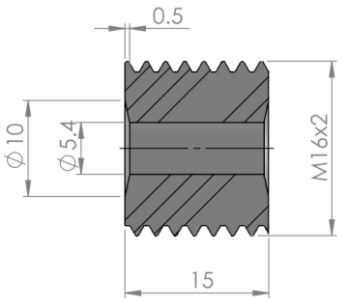

Figure 7.7 Roller

The rollers are positioned around the lead screw, making contact with it, aiming to reduce response time—a requirement of the microEDM+US machining process. Two rollers are arranged at 45˚ and are mounted first. The third roller is positioned at 7˚, and its role is to keep all the rollers in contact with the lead screw and exert a pressing force through the lever effect or contact pressure. This ensures the precision of the positioning of the feed system (**Figure 7.8**).

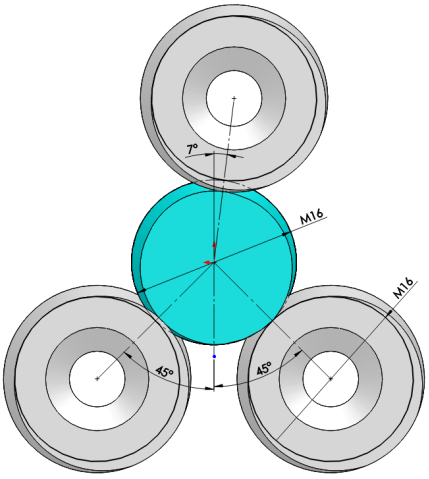

Figure 7.8 Arrangement of rollers on the lead screw

To assemble the rollers into the nut assembly (body), each roller is equipped with two cages to retain the balls, two sets of six balls to allow rotation around the roller axis with minimal friction,

and a screw for assembly into the nut body (as shown in **Figure 7.9**). Each roller has a through-hole for the M10 screw and a thread defined by the dimensions in **Figure 7.7**, necessary for mounting the ball cages.

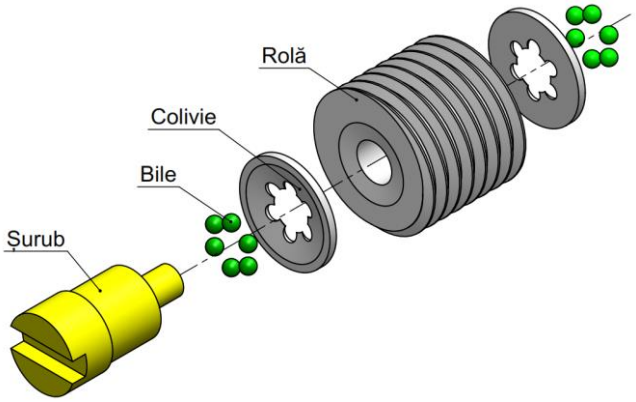

Figure 7.9 Roller subassembly

The roller subassembly from **Figure 7.9** s assembled into the nut body shown in **Figure 7.10**. The attachment of the two rollers to the nut body is achieved through the threaded M10 holes highlighted in **Figure 7.10**, nd the orientation of the rollers is controlled by the profiled support (the circular channel has the conjugate shape of the balls) assembled with interference fit (*H7/p6*) into the nut body from **Figure 7.11**.

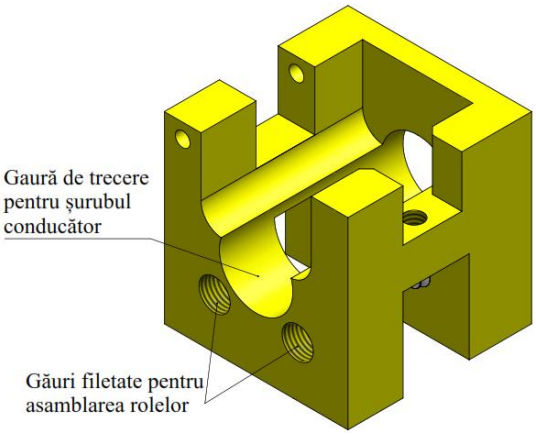

Figure 7.10 Highlighted holes used for fixing the rollers in the nut body

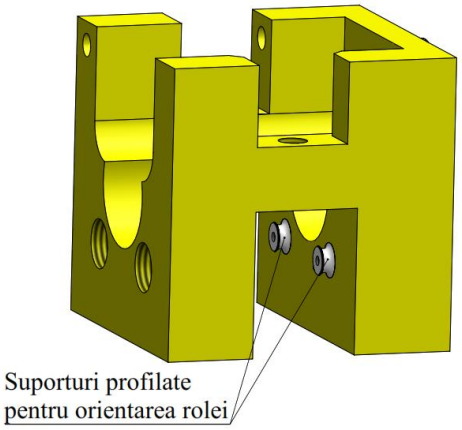

Figure 7.11 Highlighter profiled support for the orientation of the rollers in the nut body

For the assembly of the third roller, a support is needed to allow its assembly and disassembly on the lead screw (**Figure 7.12**). The assembly of the roller onto the support will be similar to that of the ones in the nut body. This support enables the use of a lever with the help of a hook, ensuring greater force to bring all the rollers into contact with the lead screw and, consequently, the precision of the positioning of the feed system. This assembly method is highlighted in **Figure 7.12**.

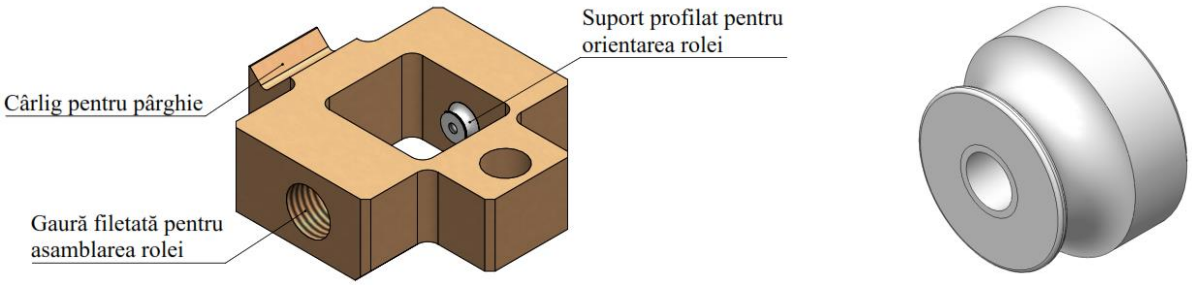

Figure 7.12 The support of the third roller (left) and the profiled support (right)

The nut should not undergo a rotational motion (in EDM, surfaces that are not of revolution are created). Therefore, it is assembled by threading with an intermediate plate featuring a guide column with a longitudinal flat surface (**Figure 7.13**). In combination with the bearing (roller) from support 2 (**Figure 7.14**), it will take over the rotational movement. Additionally, the shaft is equipped with a dowel hole used for mounting the ultrasonic chain.

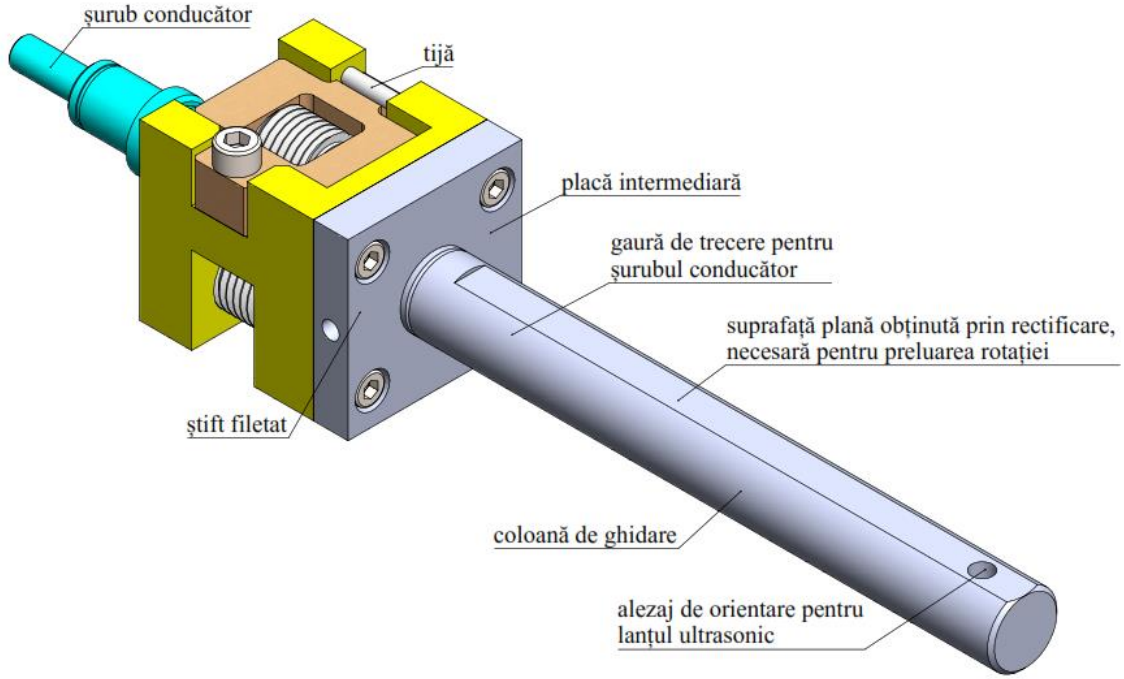

Figure 7.13 Assembly of a guide column on the nut body

The design of all other elements that form the screw-nut assembly with rollers is next.

7.4. Auxiliary elements design

In this stage, the rest of the support elements for the screw-nut system are designed. **Figure 7.14** presents the designed feed system (excluding the MPP, encoder, and US chain).

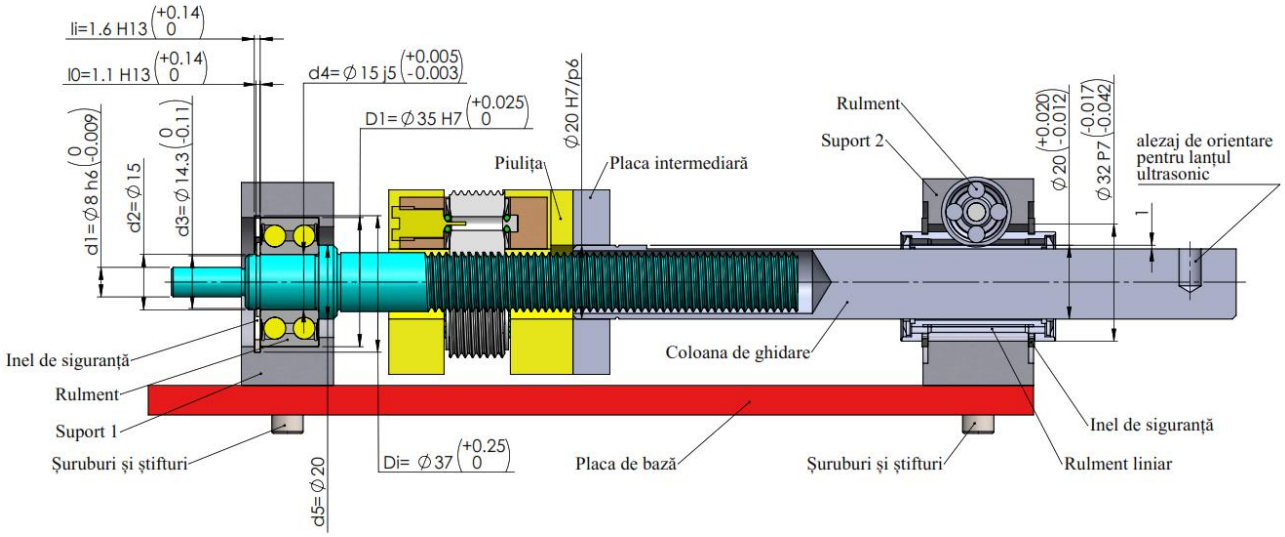

Figure 7.14 The screw-nut feed system

In the left part of **Figure 7.14** is support 1, which provides the main support surface for the lead screw. Inside, it is equipped with a bearing to reduce friction, influencing the response time for the feed and retract commands of the feed system. On the nut body, the guide column is assembled

using an intermediate plate, which prevents the rotation of the nut and transforms the rotational motion of the lead screw into translational motion. On the guide column, there is a dowel hole used for assembling the ultrasonic chain and a flat surface of 1 mm deep relative to the column circumference to block the rotation through the contact with the bearing in support 2 (**Figure 7.15**).

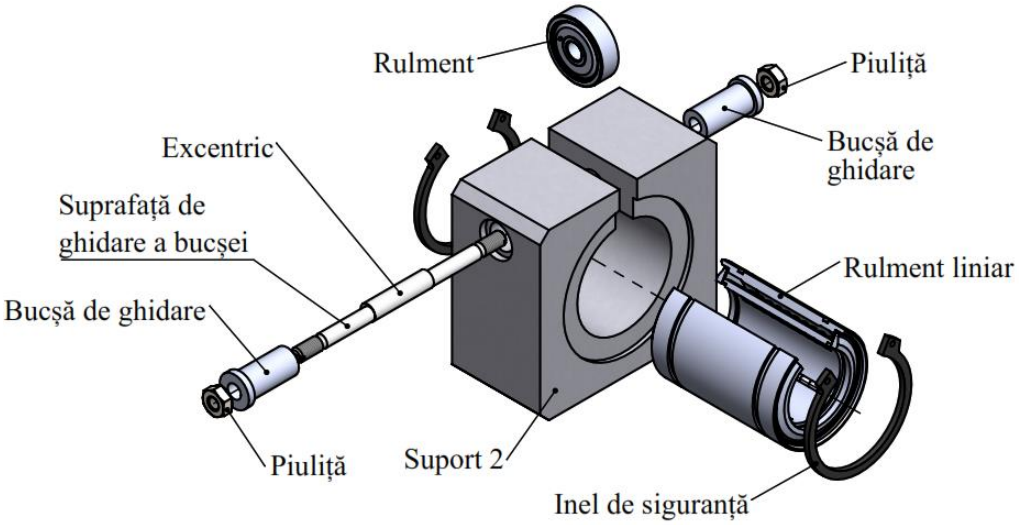

Figure 7.15 Detail for support 2

This bearing is mounted on an eccentric and inserted into support 2. Then, two guide bushings are introduced, making contact with the surface in **Figure 7.15**. When rotating the eccentric, the bearing approaches or moves away from the longitudinal flat surface of the guide column. Support 1 and support 2 are fixed and oriented on a base plate using screws and dowels (**Figure 7.14**).

In the same stage, the rotary plate that allows adjusting the perpendicularity of the feed system is designed (**Figure 7.16**). It has two circular channels, and the angular fixation is ensured through two screws with washers. The rotary plate is assembled with the base plate and with the support used for attaching the feed system to the machine tool.

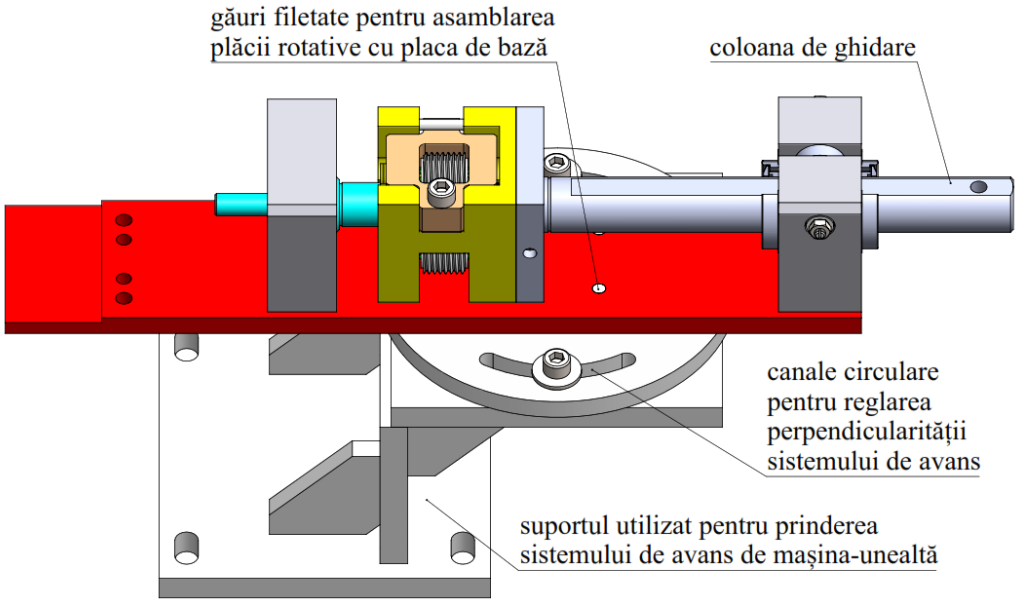

Figure 7.16 Feed system with the rotary plate for adjusting perpendicularity

The perpendicularity adjustment is achieved by probing the guide column with a comparator during its axial displacement through the MPP control.

7.5. Ultrasonic chain clamping system design

The ultrasonic chain is oriented and secured through two prisms [29], whose contact occurs in the nodal channel area of the concentrator. Minimal contact with the concentrator over a length of 12 mm was imposed as a condition to prevent the transmission of vibrations throughout the system.. The contact of the prisms with the concentrator is symmetrical to the nodal channel (the point where the amplitude is zero).

It is worth noting that the prisms are designed based on the modeling and physical realization of the concentrator.

In **Figure 7.17**, elongation is presented as a function of distance from the nodal channel. The distance from the channel is dimensioned from the tip of the concentrator. The data for creating **Figure 7.17** is extracted from the final Comsol model of the concentrator (**Figure 8.3**). The data extracted from Comsol represents the amplification factor *K*. To obtain elongation, this amplification factor *K* is multiplied by a specific amplitude (in this case, $A = 1\ \mu m$).

From **Figure 7.17**, it is evident that the zero amplitude (nodal point) is at a distance of **46.3 mm** from the frontal surface of the concentrator. Therefore, contact with the two prisms will be made over a symmetrical distance of 6 mm. The contact surface of the prisms with the concentrator is designed in the dimensional interval of 40 – 52 mm, measured from the frontal surface of the concentrator.

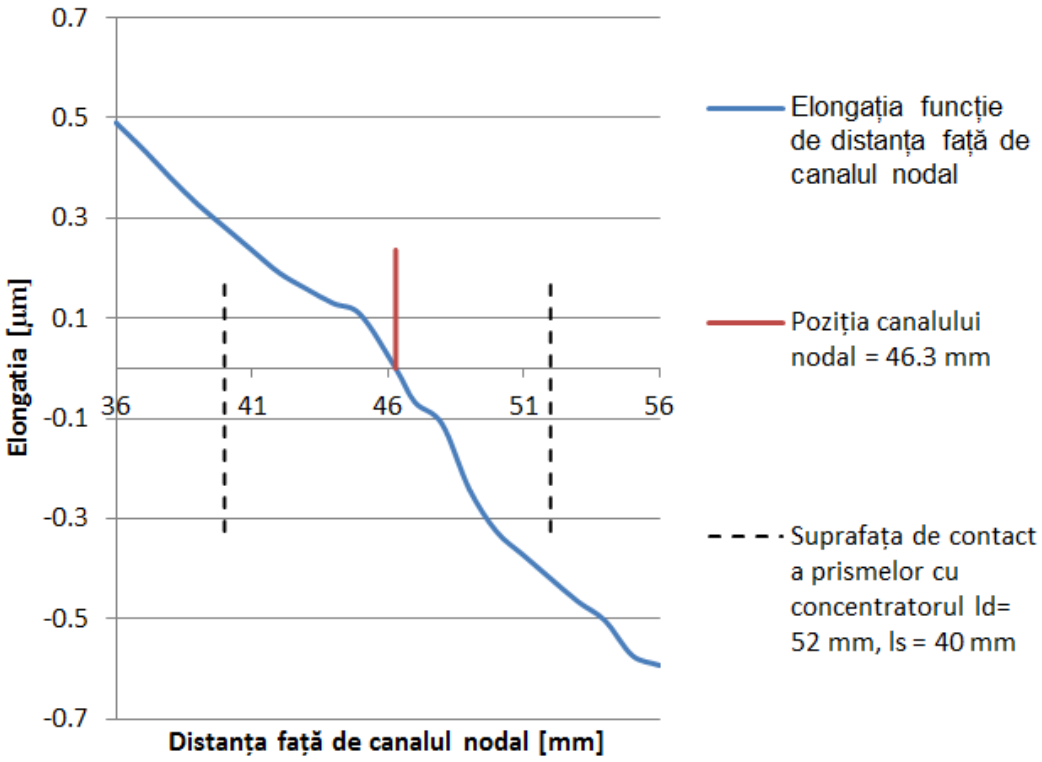

Figure 7.17 Variation of elongation with respect to the distance from the nodal channel

To assist in centering the nodal channel in the middle of the prisms, a threaded conical pin (**Figure 7.18**) is inserted into one of the prisms.

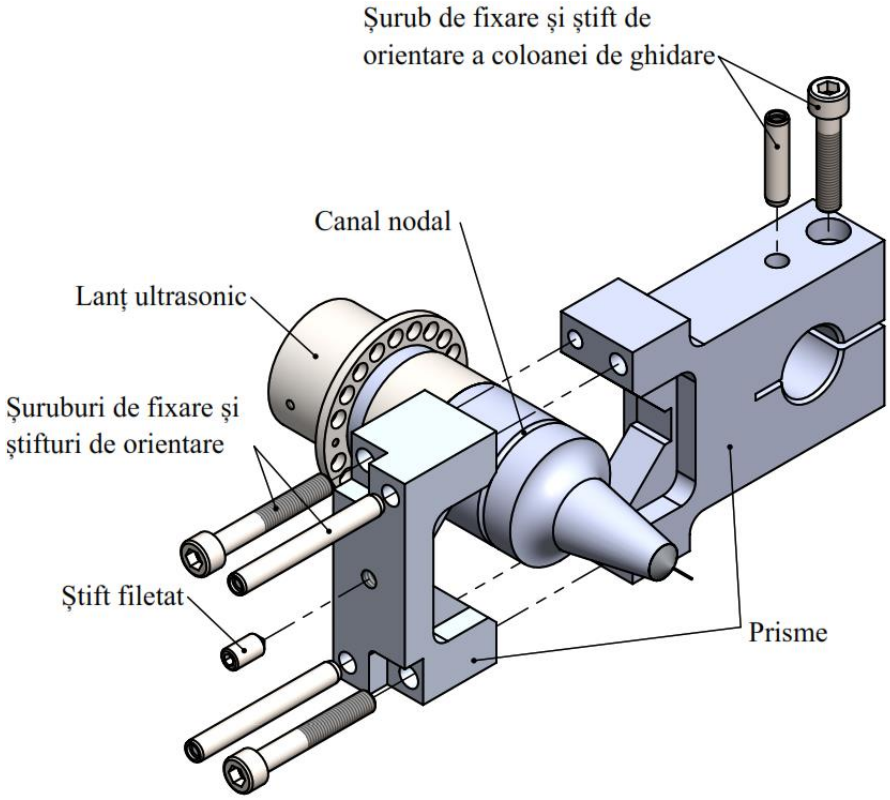

Figure 7.18 Assembly of the concentrator with the prisms

The cone of the pin will center the nodal channel of the concentrator in the middle of the prisms, and the fixing screws will be tightened, ensuring the orientation and securing of the ultrasonic concentrator with the help of the prisms. The prisms are made of AlZnMgCu15 (aluminum alloy) to minimize the load on the feed system. The total mass of the assembly in **Figure 7.19** is **0.949 kg**, corresponding to an axial load of approximately *Fa = 10 N*. The condition is that the mass of the assembly does not exceed 1 kg (see subchapter 7.1.1).

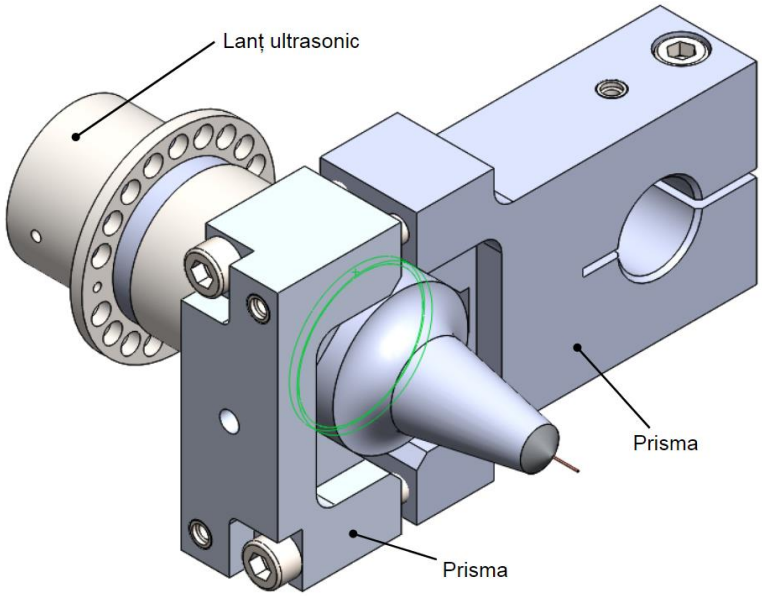

Figure 7.19 Assembly of the concentrator along the nodal channel (green) with the ultrasonic chain.

The prisms are oriented and secured to each other by two *M6* screws and two *Ø6 h6* pins. A *Ø6 h6* orientation pin and an *M6* screw are used to guide and secure the ultrasonic chain to the guide column through tightening with an elastic bore (**Figure 7.18**).

Chapter 8. Modeling and Simulation of the Operation of the Feed System for Ultrasonic Assisted Microelectroerosion

8.1. Modeling and simulation of the ultrasonic concentrator

The Comsol Multiphysics program with the Structural Mechanics module and the Eigenfrequency study is used to model the ultrasonic concentrator designed in chapter 7.5 [39]. The material used is AISI 4340 steel for the concentrator and 99.5 copper for the wire EDM tool. The geometry of the ultrasonic concentrator is created in 2D axisymmetric space, using parameters from **Table 8.1**. The lengths and radii of the concentrator were taken from Chapter 7.5, where the initial design of a step cylindrical concentrator was done.

Table 8.1 Parameters of the initial stage concentrator

Parameter	Expression	Value	Description
l1	33.372 [mm]	0.033372 m	upper step length
r1	17.5 [mm]	0.0175 m	upper step radius
l2	35.596 [mm]	0.035596 m	lower step length
r2	10 [mm]	0.01 m	lower step radius
rr	r1-r2	0.0075 m	radii between diameter steps
modulE	2.1E11	2.1E11	Young AISI 4340 module

Figure 8.1 depicts the eigenfrequency of the concentrator f_{cr} = *36078 Hz* and the amplification *K = 2.96*, the maximum value of the ratio between the elongation at the input section (considered *K=1*) and output of the concentrator.

To achieve the target frequency of 40805 Hz from the initial frequency of 36078 Hz, the concentrator will go through a series of adjustment stages, involving modifications to its geometry and, consequently, changes in frequency and amplification coefficient.

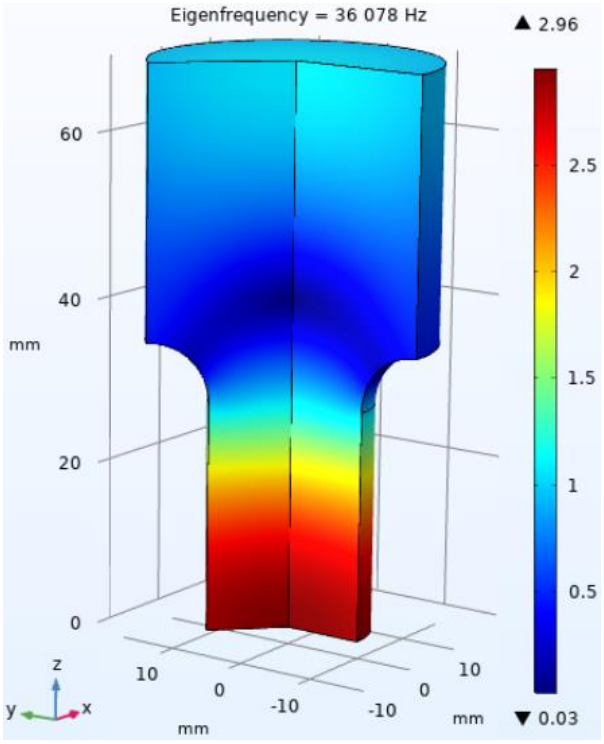

Figure 8.1 Eigenfrequency and amplification in the initial stage of the concentrator

Figure 8.2 depicts the concentrator with the nodal channel, featuring a natural frequency of 40909 Hz and an amplification factor of 2.7.

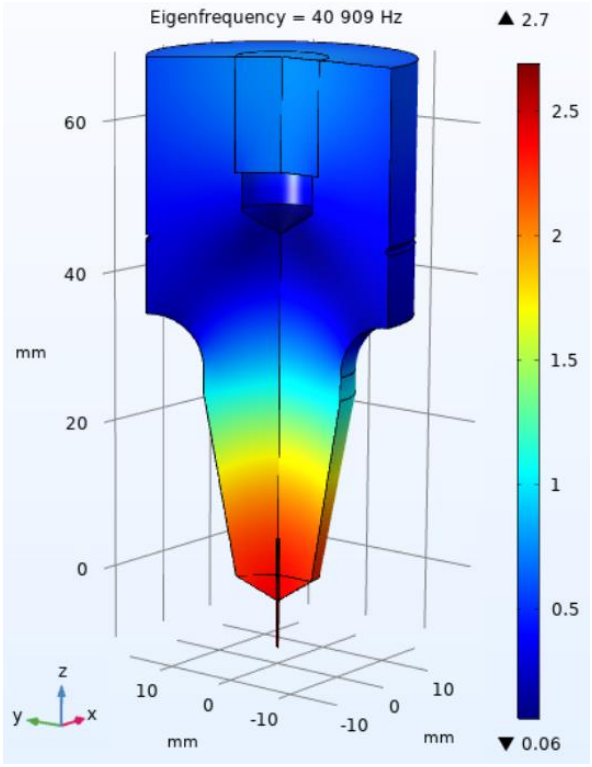

Figure 8.2 Eigenfrequency and amplification in stage 5 of the concentrator

8.1.1. Concentrator adjustement to reach target eigenfrequency

Since the natural frequency in stage 5 of the concentrator, f_{cr} = *40909 Hz*, s higher than the target frequency, f_{tr} = *40805 Hz*, adjustments to the concentrator are required by modifying the dimensions l_1 and l_2. Increasing the dimensions of l_1 and l_2 results in a decrease in the eigenfrequency of the concentrator, and vice versa.

Table 8.2 illustrates the modifications made to reach the target frequency.

Table 8.2 Variation of the concentrator's natural frequency as a function of length

Upper step length l_1 [mm]	**Lower step length l_2 [mm]**	**Concentrator eigenfrequency f_{cr} [Hz]**
33.372	*35.596*	*40909*
33.472	35.696	40803
33.572	35.796	40698
33.672	35.896	40593
33.676	35.9	40589
33.776	36	40485
33.5	36	40557
33.6	36	40531
33.7	36	40505

It is observed that the target frequency is achieved for the values l_1 = *35.696 mm* and l_2 = *33.472 mm* (highlighted in green). However, the concentrator has been modeled virtually, therefore these values cannot be adopted in practice as they do not allow for length adjustment after physical processing.

For this reason, the values l_1 = *36 mm* and l_2 = *33.5 mm* are chosen (highlighted in orange), which ensure a natural frequency of 40557 Hz and allow adjustment through processing (from l_1)

to the target frequency of 40805 Hz. Due to the length changes, the nodal channel has been repositioned at a distance of 46.3 mm without altering the eigenfrequency. The parameters of the final concentrator are presented in **Table 8.3**.

Table 8.3 Parameters of stage 6 of the concentrator

Parameter	Expression	Value	Description
l1	36 [mm]	0.036 m	upper step length
r1	17.5 [mm]	0.0175 m	upper step radius
l2	33.5 [mm]	0.0335 m	lower step length
r2	10 [mm]	0.01 m	lower step radius
rr	r1-r2	0.0075 m	radii between diameter steps
modulE	2.1E11	2.1E11	Young AISI 4340 module
alfa	1 [º]	1º	inclination degree
rgaurasc	0.2 [mm]	2E-4 m	housing radius of tool electrode
hgaurasc	5 [mm]	0.005 m	housing depth of tool electrode
lscula	15 [mm]	0.015 m	electrode length
modulECu	130 [GPa]	1.3E11 Pa	Young Cu module
hlipire	3.5 [mm]	0.0035 m	height of silver welding seam
modulEAg	69 [GPa]	6.9E10 Pa	Young Ag module
rgaura	5.1 [mm]	0.0051 m	hole radius
hgaura	20 [mm]	0.02 m	hole depth
rfilet	6 [mm]	0.006 m	thread radius
hfilet	15 [mm]	0.015 m	thread depth
beta	59 [º]	59º	tip tilt
rcanal	0.5 [mm]	0.005 m	nodal channel radius
zcanal	46.3 [mm]	0.0463	z coordinate for nodal channel

Figure 8.3 illustrates the model of the final concentrator with an eigenfrequency f_{cr} = 40557 Hz and an amplification factor K = 4.62. To achieve the target f_{tr} = 40805 Hz, the concentrator will be tested and processed sequentially. The model is then imported into Solidworks and integrated into the feed system assembly. The concentrator's mass is 0.304 kg.

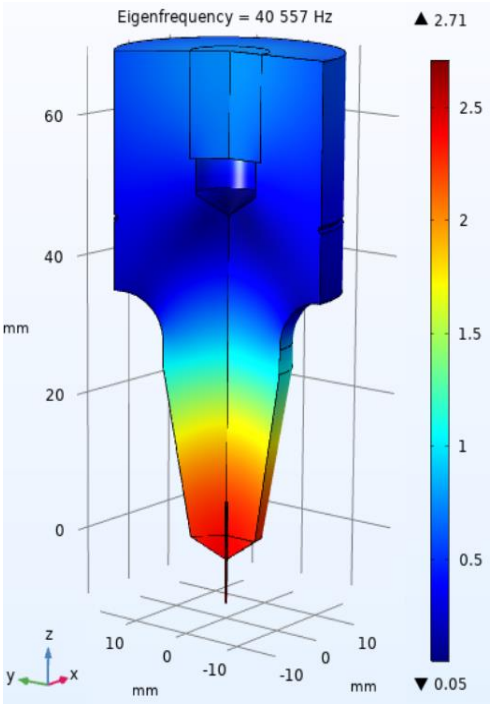

Figure 8.3 Eigenfrequency and amplification in stage 6 (final) of the concentrator

For assembling the concentrator with the IMSAR transducer, an M12 bolt (**Figure 8.4**) with a length of 18 mm is used, made of the same material as the concentrator - AISI 4340 steel. The mass of the bolt is 0.012 kg.

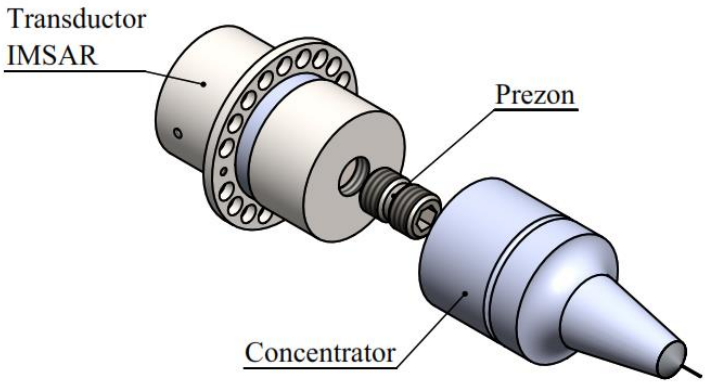

Figure 8.4 Assembly of the transducer with the concentrator using a bolt

8.2. Numerical simulation of the feed system's eigenfrequency

Natural frequencies, or eigenfrequencies, are specific discrete frequencies at which a part or a system is prone to vibrations. If a system is subjected to an external periodic force with a frequency equal to or close to one of the eigenfrequencies of the system or its components, it begins to exhibit vibrations with relatively large amplitudes. This equality of frequencies is referred to as resonance [32].

The tool electrode is ultrasonically assisted, vibrating with an amplitude between 1 – 2 μm, so any additional vibration induced by resonance affects the stability of the process [33].

Under these conditions, a study was conducted to observe if the lead screw resonates with the frequency of the motor control system [30] (**Figure 8.5**).

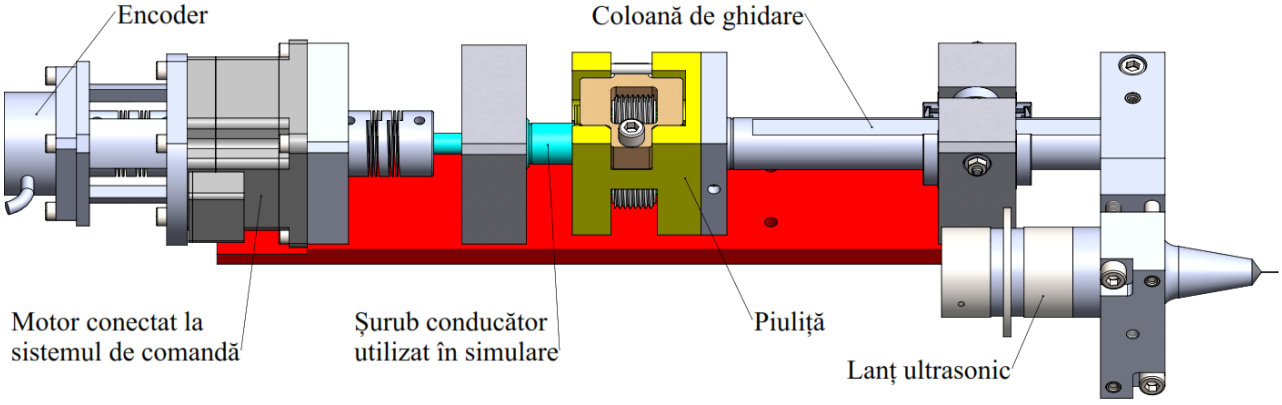

Figure 8.5 The assembled feed system for ultrasonic assisted microelectroerosion

8.2.1. Determination of the frequencies used by stepper motor control system

To determine the frequencies to which the lead screw is subjected, the MPP diagram from **Figure 8.6** is used. The motor system is driven with maximum torque to ensure maximum rotor acceleration, essential for minimizing response time.

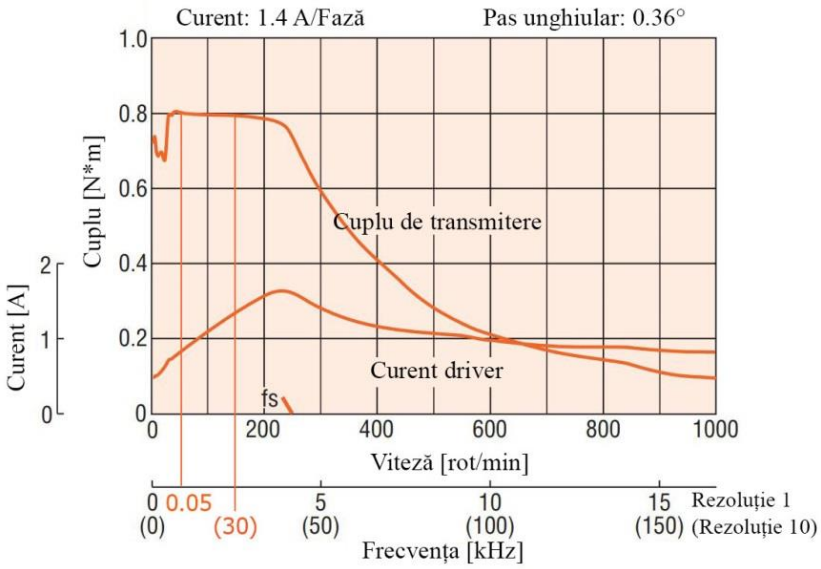

Figure 8.6 Speed – Torque characteristics for MPP [21]

According to **Figure 8.6**, the frequency range required for the motor to operate at maximum torque is between 0.05 – 30 kHz. Using the limiting frequencies, the maximum and minimum speeds of the feed system are calculated using the following formulas:

$$v_{max} = i * f_{max}\ [mm/s] \qquad \textbf{(8.1)}$$

$$v_{min} = i * f_{min}\ [mm/s] \qquad \textbf{(8.2)}$$

where: i – inear increment of the feed system [mm]; f_{max} – maximum frequency of the pulses [Hz]; f_{min} – minimum frequency of the pulses [Hz];

At each pulse, a displacement is made with a linear increment of 0.2 µm, the maximum frequency is 30000 Hz, and the minimum frequency is 50 Hz. Substituting into formulas **(8.1)** and **(8.2)** yields the maximum and minimum speed of the feed system:

$$v_{max} = 2 * 10^{-4} * 30000 => v_{max} = 6\ mm/s => \boldsymbol{v_{max} = 360\ mm/min}$$

$$v_{min} = 2 * 10^{-4} * 50 => v_{min} = 0.01\ mm/s => \boldsymbol{v_{min} = 0.6\ mm/min}$$

The stepper motor, controlled by the programmed software, accelerates and decelerates using an "S"-shaped speed profile (**Figure 8.7**), as a precautionary measure against shocks induced by abrupt movements.

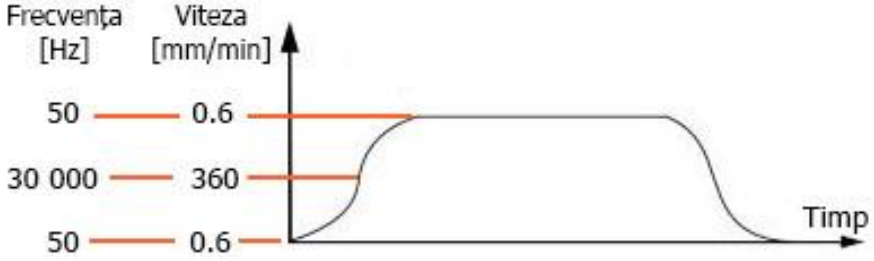

Figure 8.7 „S"-shaped speed profile used for MPP displacement

During the microEDM+US process, the control system utilizes a frequency of 50 Hz. In case of a short circuit or open circuit, the displacement is carried out as follows: it starts with an acceleration corresponding to the frequency of 50 Hz up to 30000 Hz (inflection point), after which a deceleration follows, corresponding to the frequency of 50 Hz, as seen in **Figure 8.7**.

The speed profile indicates that the most commonly used actuation frequency for MPP is 50 Hz, serving as a plateau value. The frequencies used for the "S" profile are transitory, and around the inflection point, they are close to the maximum value of 30000 Hz.

8.2.2. Eigenfrequency simulation

The simulation is carried out in Comsol Multiphysics, using the Solid Mechanics module with the Eigenfrequency study.

Considering that the minimum frequency is 50 Hz, six frequencies around this nominal value are sought, and the result is presented in **Figure 8.8**:

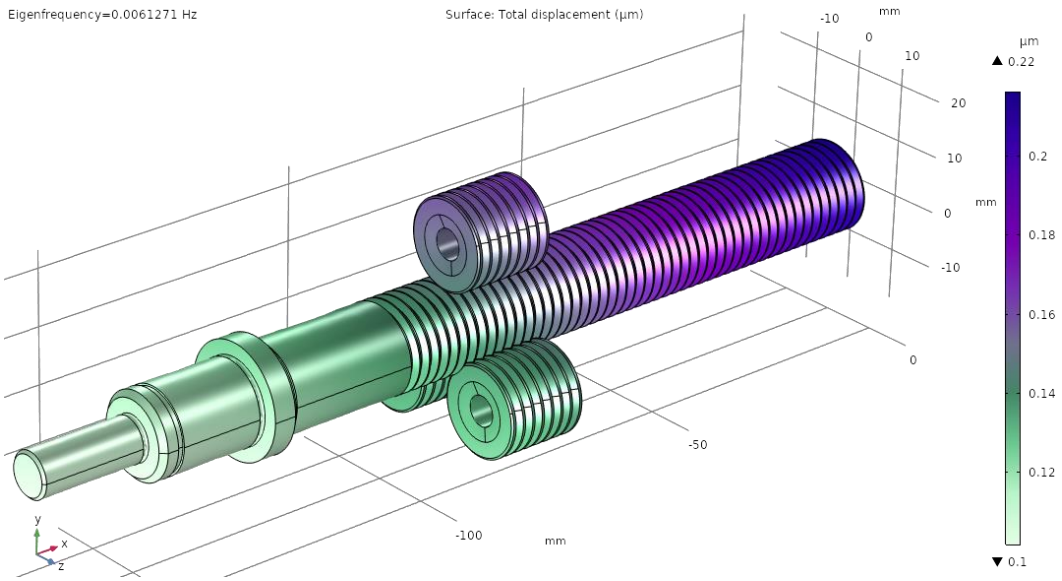

Figure 8.8 The resulted model from the study, where the eigenfrequency of the lead screw is 0.00612 Hz at the nominal value of 50 Hz

The position of the three rollers is not fixed, being parameterized. Therefore, for the study to be relevant, the eigenfrequency must be tested when the rollers are in different positions, as shown in **Figure 8.9**.

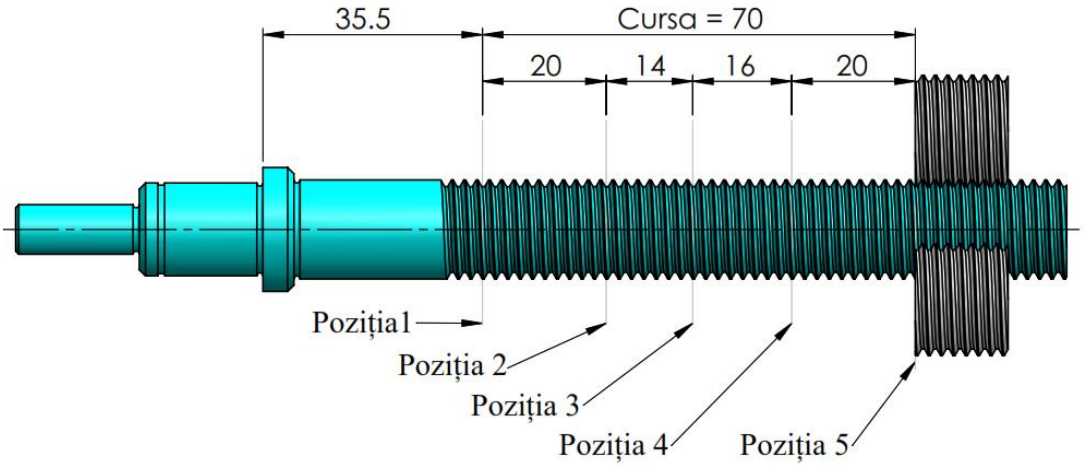

Figure 8.9 Lead screw with rollers in different positions

8.2.3. Results

Figure 8.10, illustrates, for example, the result obtained for position 3 and the target nominal frequency of 50 Hz.

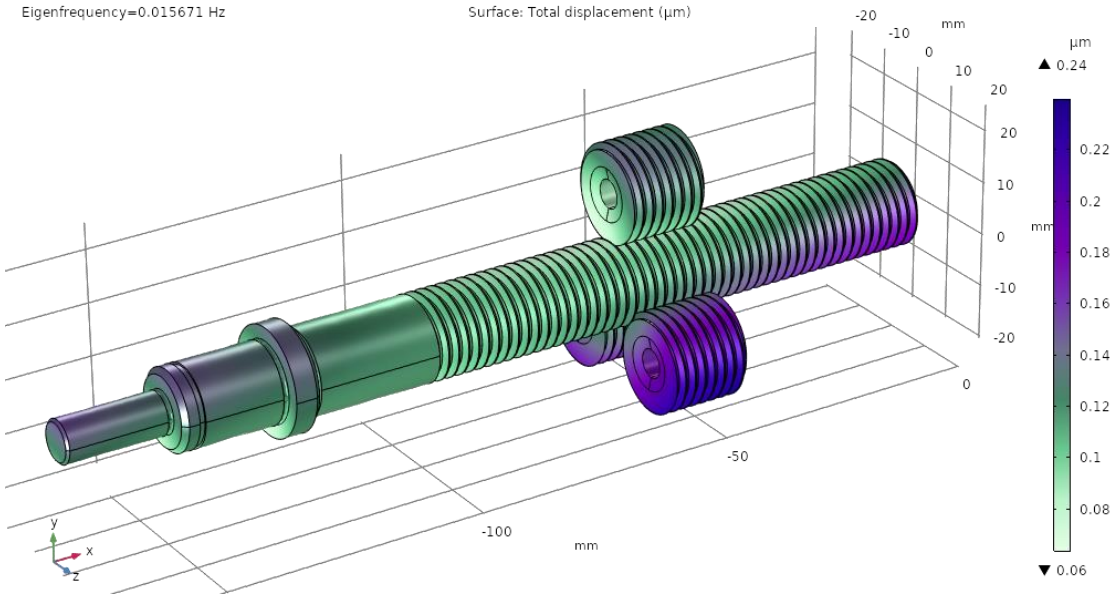

Figure 8.10 The resulting model from the study (position 3), where the natural frequency of the lead screw is 0.01567 Hz

The results for each frequency corresponding to the defined positions above are presented in **Table 8.4**. These show that the feed system does not resonate with the operating frequency of the stepper motor at this operating regime. Moreover, for the testing frequency of 30000 Hz, the difference is over 100 Hz.

An exception is position 5, at the testing frequency of 30000 Hz, where the difference between frequencies is very small (15 Hz). This would imply that the feed system executes a displacement (advance or retract) at maximum speed at the end of the stroke, which is not possible. Considering that the positions are transitory, it can be said that the feed system does not enter resonance.

Following the tests regarding the response time of the feed system, the utility of the MPP command with a frequency of 1000 Hz was observed. Therefore, it is of interest to study the eigenfrequency of the screw-nut system around this value.

The study settings are adjusted to 1000 Hz, and the eigenfrequency is determined in the five roller positions. The results are presented in **Table 8.4**.

Table 8.4 Eigenfrequencies obtained in numerical simulations

Test frequency [Hz]	**Eigenfrequency [Hz]**				
	Position 1	**Position 2**	**Position 3**	**Position 4**	**Position 5**
50	0.00561	0.00361	0.00606	0.00619	0.00426
	0.00612	**0.00948**	**0.01567**	**0.01363**	**0.00919**
Difference [Hz]	*49.99*	*49.99*	*49.98*	*49.98*	*49.99*
1000	**1898**	**0.01038**	**0.01028**	**0.01274**	**2014**
	1962	1906	1988	2075	2085
	2418	1970	2078	2273	2251
	2643	2412	2390	2325	2528
Difference [Hz]	*898*	*999*	*999*	*999*	*1014*
30000	26776	24686	27266	26712	25480
	29067	26494	28098	**30321**	27224
	30108	29226	28817	31483	29321
	30685	**30283**	**30350**	31791	**29985**
	32017	32796	30867	32218	33455
	33240	33589	32847	32987	33976
Difference [Hz]	*108*	*283*	*350*	*321*	***15***

It is considered that the considered positions are transient, and consequently, the values of these natural frequencies of the screw-nut system are also transient. Additionally, on the "S"-curved speed profile of the feed system, the frequency value corresponds to the inflection point, which is also transient. It is assumed that the maximum static load of 10 N, displaced by the feed system, acts in the direction of reducing its eigenfrequency. Therefore, it can be stated that it does not resonate with the driving frequency of the MPP under the specified operating conditions, according to the data from **Table 8.4**.

8.3. Modeling and simulation of lead screw deformations

Deformation refers to the change in size or shape of an object under a certain load. In this study, the deformation of the threads of the lead screw under the pressure exerted by the nut is analyzed (**Figure 8.11**). The numerical simulation methodology follows several steps, which are presented below [31].

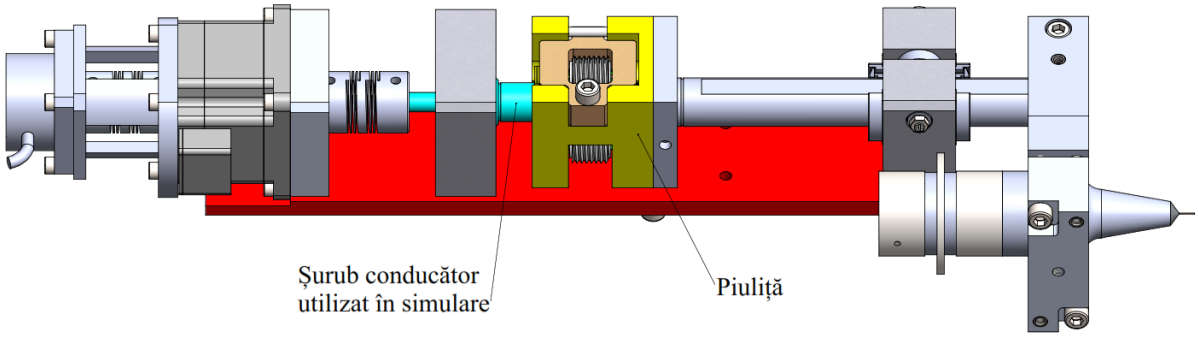

Figure 8.11 Feed system for ultrasonic aided microelectroerosions in the simulated configuration during operation

8.3.1. Determination of contact surfaces

To determine the deformation of the lead screw threads, contact surfaces need to be constructed. **Figure 8.12** shows that in the nut body, three M16x2 rollers are mounted, which are the only parts that come into contact with the lead screw threads.

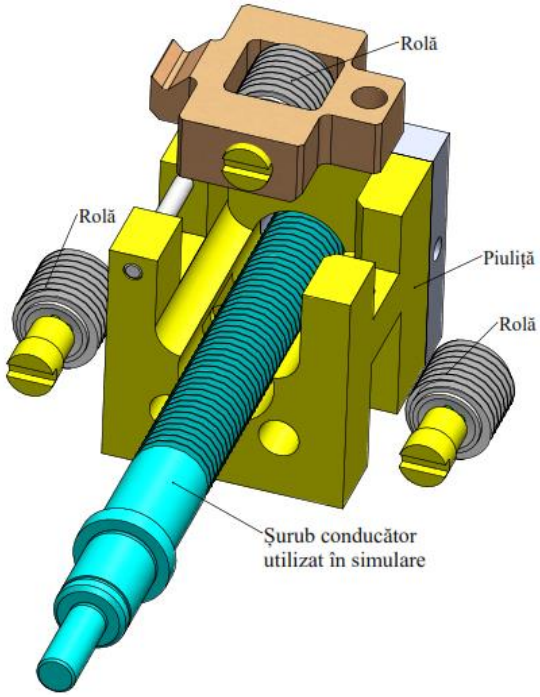

Figure 8.12 Roller screw assembly

In **Figure 8.13**, he position of the rollers relative to the lead screw is illustrated. It can be observed that two of them are symmetrically placed at an angle of 45º while one is positioned above at 7º (the angle formed by the vertical and the line containing the geometric center of the lead screw section and the roller).

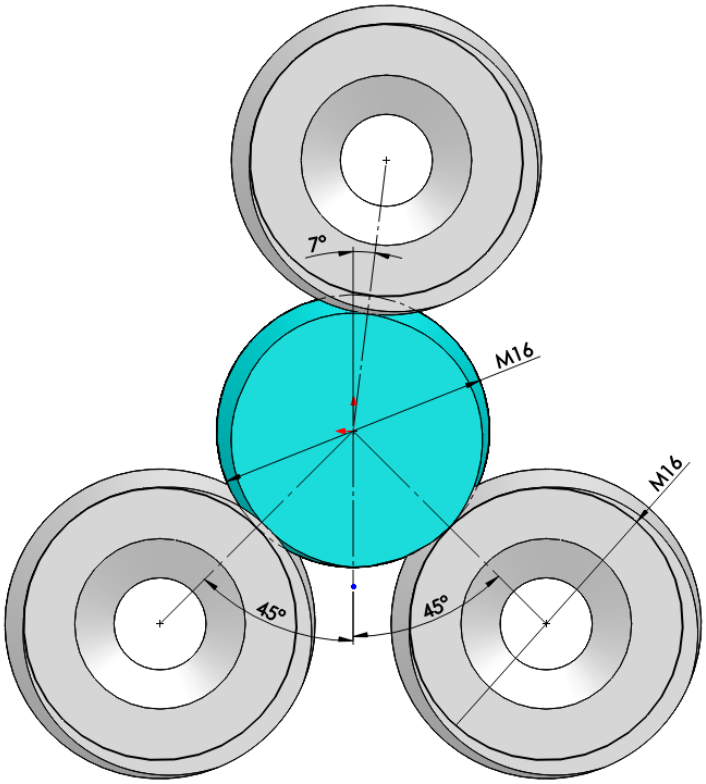

Figure 8.13 Position of the rollers relative to the lead screw

To simulate the deformation of the screw threads in different positions of the rollers, two additional sets of isolated contact surfaces are needed. The "*Lpattern*" command is used to create position 2 (40 mm) and position 3 (70 mm) from **Figure 8.14**.

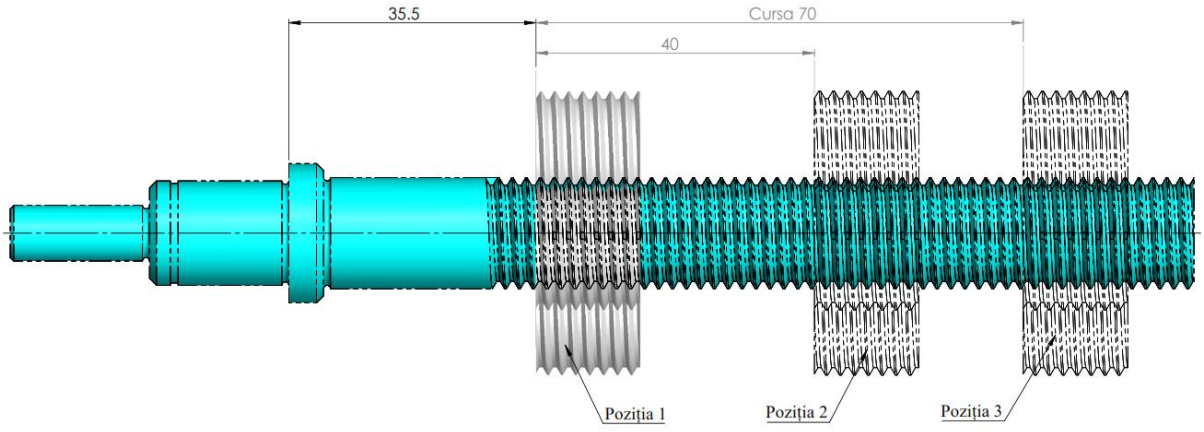

Figure 8.14 Multiple positions for deformation simulation

8.3.2. Deformation simulation

The model of the lead screw is exported from Solidworks (where it was created) and imported into Inventor, where the simulation was conducted. **Figure 8.15** illustrates the lead screw with the highlighted isolated surfaces representing the contact surfaces with the rollers in various positions.

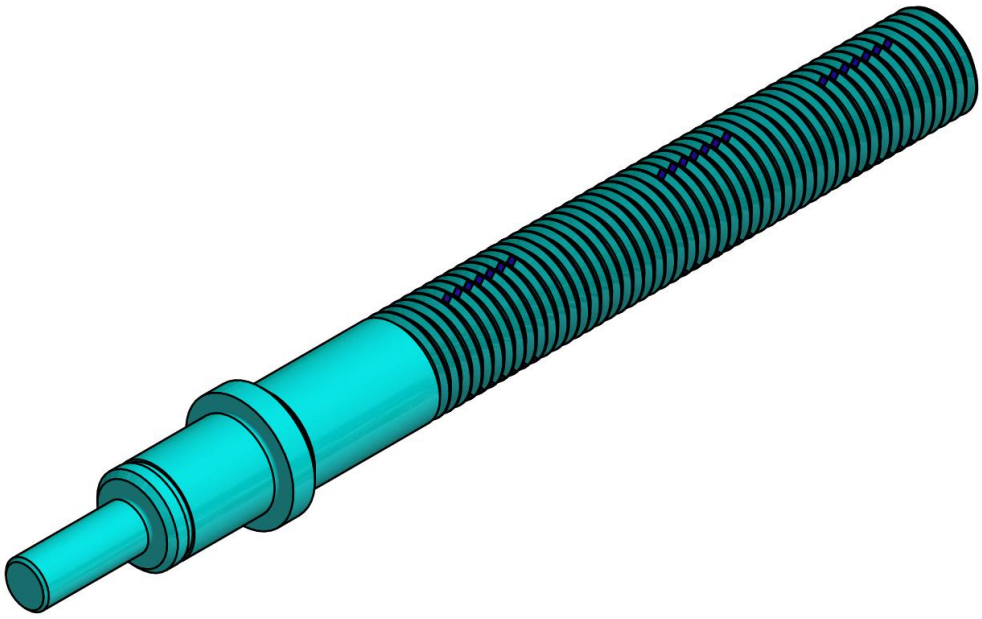

Figure 8.15 Lead screw with the contact surfaces of the rollers in three positions

The isolated surfaces in position 1 (see **Figure 8.14**) have loads (forces) applied. The mass of the nut body with all assembled parts (ultrasonic chain, nut body, guide column, prisms, etc.) is estimated at 1 kg. Multiplying the mass by the gravitational acceleration, *9.81 m/s*^{2}, results in a force of *9.81 N*, approximated to a rounded value of *F = 10 N*, which is used in the simulation.

8.3.3. Results

Results of the numerical simulation are presented in **Figure 8.16** illustrating the deformation along the X-axis. The maximum deformation is 2.363e-05 mm, which is equivalent to 0.02363 µm.

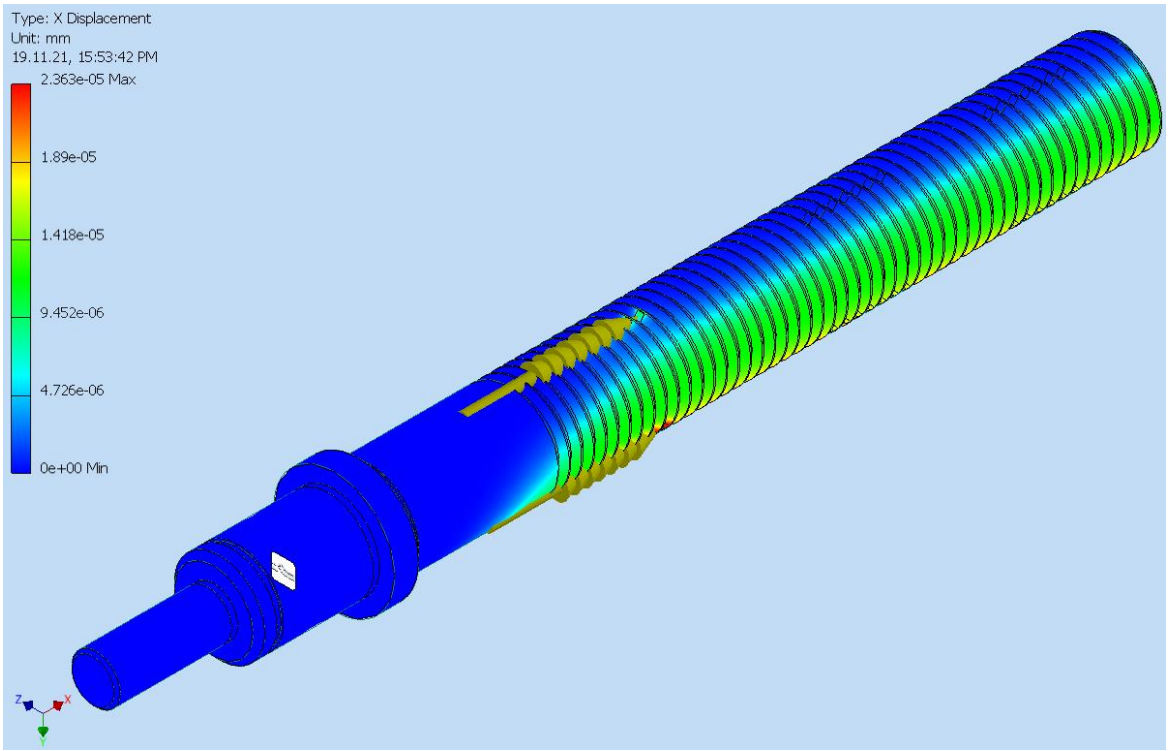

a) The deformation corresponding to roller 1 positioned at 7°

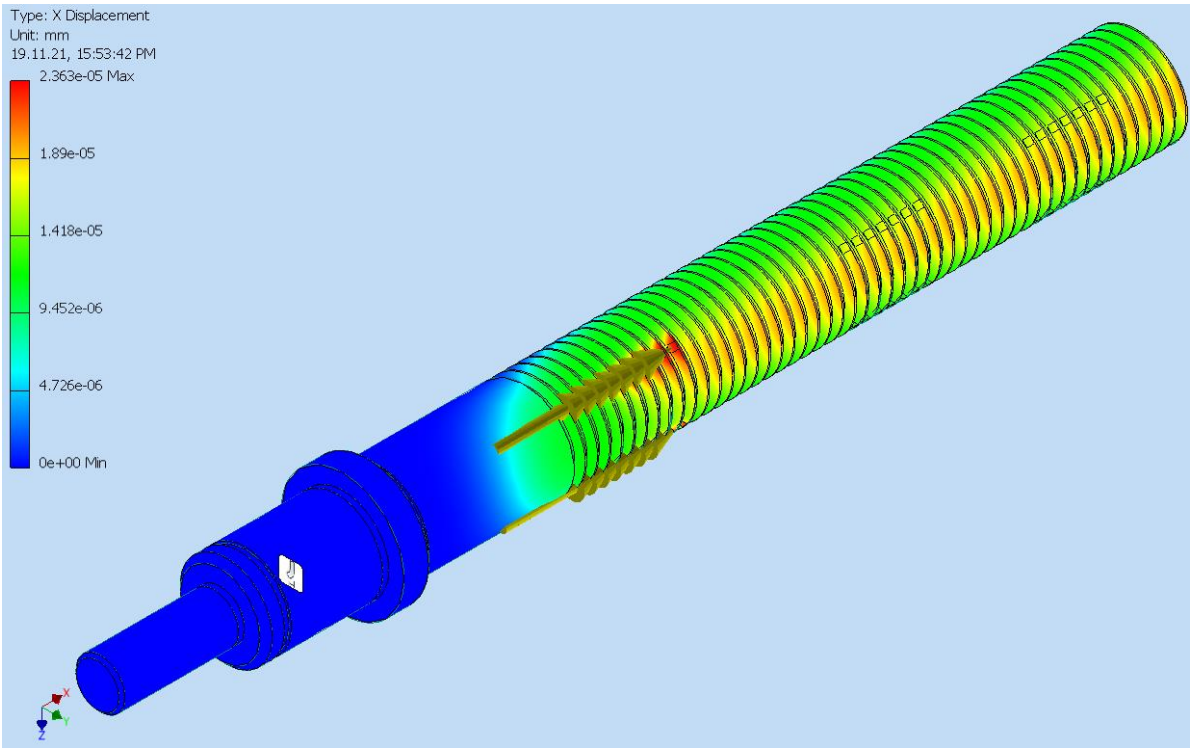

b) The deformation corresponding to rollers 2 and 3 positioned at 45°

Figure 8.16 Deformation along the X-axis

It can be observed that the deformation is not evenly distributed, due to the rollers not being positioned at equal angles around the circumference. Therefore, the deformation is higher in the area of the two rollers positioned at 45º. For comparison, numerical simulation is performed for an identical lead screw but with rollers arranged at equal angles of 120º around the circumference, showing different results for the same positions of the rollers along the working length (**Figure 8.17**).

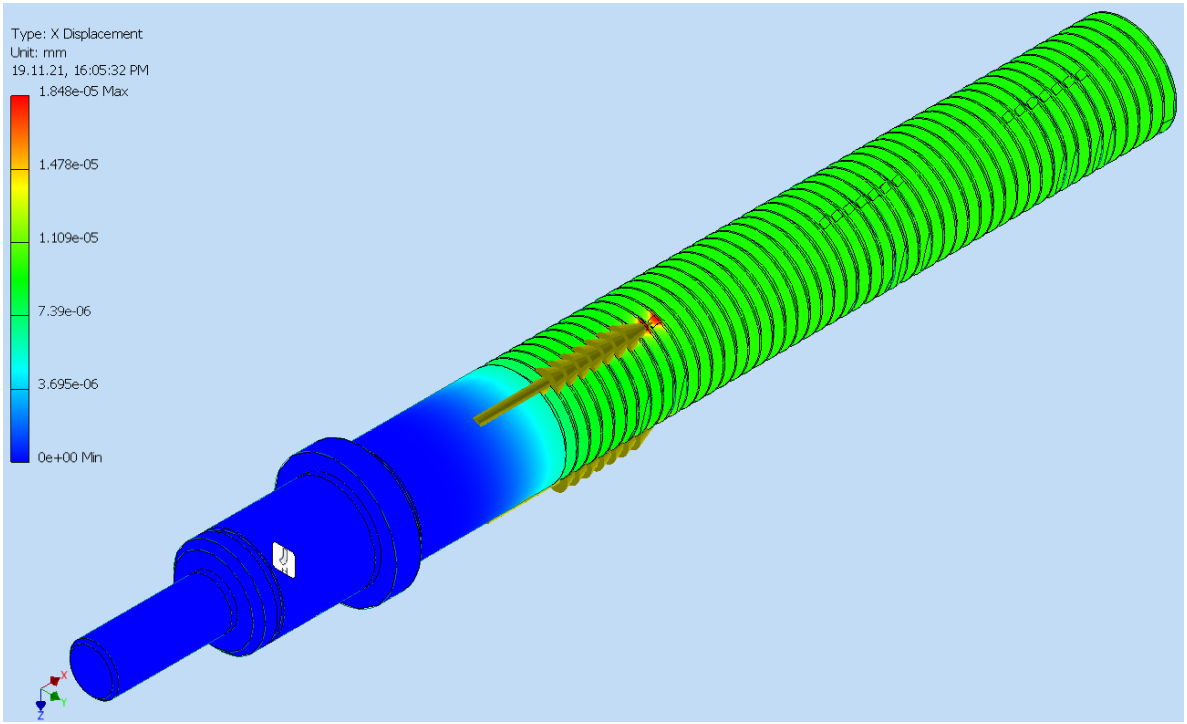

Figure 8.17 Deformation along the X-axis of the lead screw with rollers positioned at equal angles of 120°

The deformations obtained according to **Figure 8.16** are very small compared to the 0.2 µm resolution of the advance system. The advantage of this design variant is that the upper roller, positioned asymmetrically at an angle of 7°, acts like a lever, exerting a greater pressing force than in the variant with three rollers arranged at equal angles around the circumference. The deformation results for the designed lead screw are presented in **Table 8.5**.

Table 8.5 Maximum deformation along the X-axis

Position	Dimension relative to the start of the stroke [mm]	Maximum deformation [µm]
1	0	0.02363
2	40	0.04221
3	70	0.05727

The maximum deformation in the case of the designed lead screw is 0.057 µm, as obtained from numerical simulation, so it can be assumed that the deformation has a minimal impact on the stability and precision of the machining.

The results of numerical simulation regarding the deformation of the lead screw with the rollers arranged at an angle of 120° are presented in **Table 8.6**.

Table 8.6 Maximum deformation along the X-axis for the lead screw with rollers at 120°

Position	Dimension relative to the start of the stroke [mm]	Maximum deformation [µm]
1	0	0.01848
2	40	0.03116
3	70	0.0408

Additionally, a smaller deformation is observed in the case of rollers arranged at 120°, 0.041 µm compared to the previous variant 0.057 µm, the resulting values being an order of magnitude smaller in relation to the resolution of the feed system.

Chapter 9. Design of the Technological Process, Fabrication and Testing of the Feed System

9.1. Test of the ultrasonic concentrator

The designed and manufactured ultrasonic chain has been tested under laboratory conditions, reaching a technological maturity level of 4 - TRL 4.

The ultrasonic chain, which includes the tool-electrode for micro-holes, is connected to an oscilloscope and a variable-frequency signal generator - **Figure 9.1**.

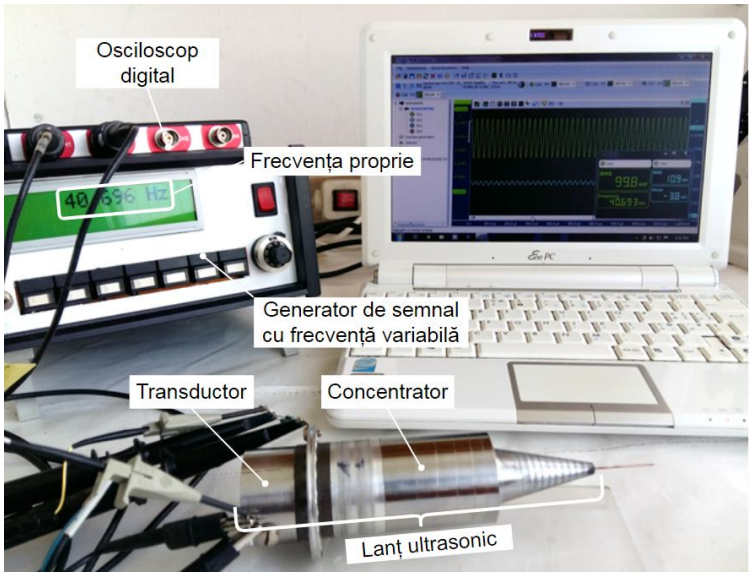

Figure 9.1 Experimental setup for determining the eigenfrequency of the physical concentrator

It is mentioned that for high-quality PZT transducer, the difference between series and parallel resonance frequencies should be at least 1-2 kHz (a condition met in this case). Also, at series resonance (used in this case), the voltage on channel CH2, displayed on the oscilloscope screen, should be minimal – **Figure 9.2**, while at parallel resonance, the voltage should be maximal.

Figure 9.2 Detail of the digital oscilloscope screen with the determination of the resonance frequency at 40693 kHz

The determined natural frequency of the physical concentrator is 40696 Hz, compared to the simulated natural frequency of the concentrator at 40557 Hz. A difference between the physical and simulated models is observed, as physical manufacturing introduces factors such as deviations in chemical composition, material in homogeneities, dimensional and shape variations in the junction surfaces of components, etc.

Adjustments (reductions) were made to the length of the upper step of the ultrasonic concentrator (the only one available after assembling the filamentary tool electrode), and iterative tests were conducted to achieve the target frequency of 40805 Hz.

Within the same experimentation, the cavitation phenomenon was also tested at the tip of the ultrasonic chain, where the filamentary tool electrode for EDM+US micromachining is located, by immersing it in water and connecting the ultrasonic chain to a ultrasonic generator with a nominal frequency of 40 kHz - designed by Mr. Engineer Ștefan Nițișor - which resonated at the series resonance frequency, as shown in **Figure 9.3**.

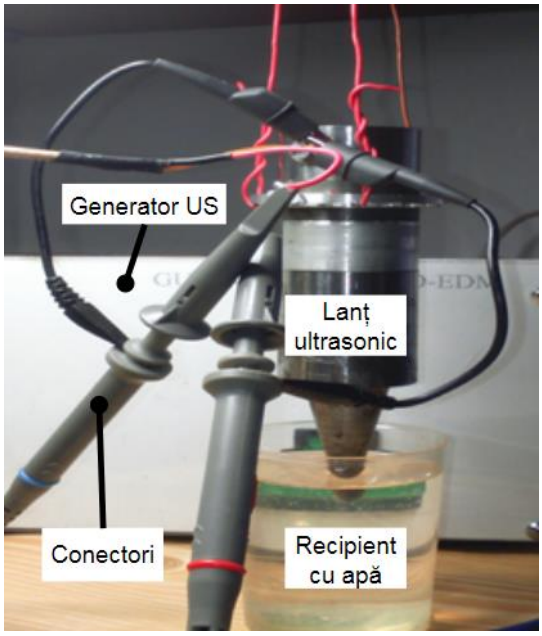

Figure 9.3 Ultrasonic cavitation test

During operation, cavitation bubbles were observed at the end of the ultrasonic chain, confirming its proper functioning.

9.2. Test of the feed system's movement

The feed system was tested regarding the execution mode of movements in laboratory conditions (level 4 technological maturity - TRL4) at the Faculty of Electronics, Telecommunications, and Information Technology (ETTI), the Center for Technological Electronics and Interconnection Techniques (CETTI) within the Polytechnic University of Bucharest. The experiments were conducted under the guidance of engineer Gheorghe Jitianu from EDMING SERV SRL and Assoc. Prof. Dr. Eng. Andrei Drumea from the ETTI faculty. These tests also aimed to validate the feed system's models and simulations presented earlier. The testing stand for the feed system is shown in **Figure 9.4**

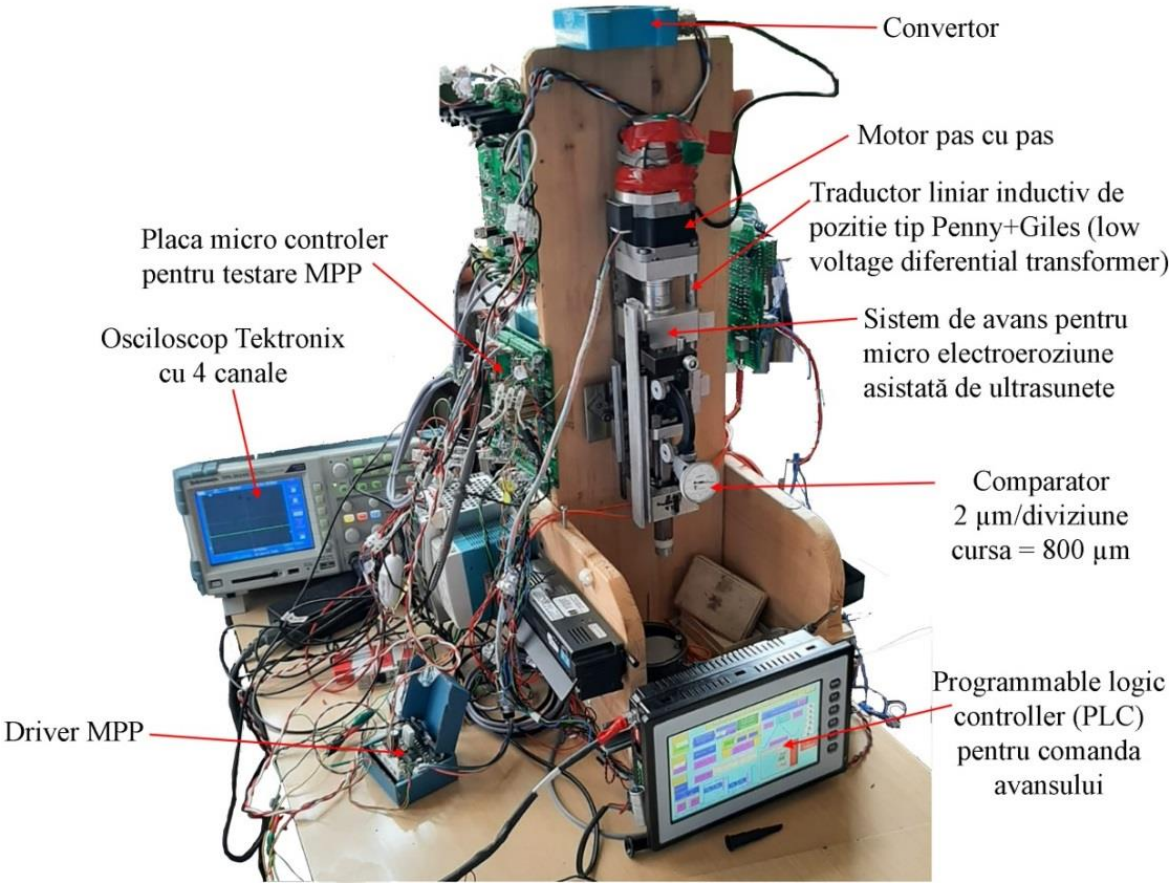

Figure 9.4 Testing stand for the feed system

In this subsection, the prototype of the microEDM+US feed system will be tested, aiming to observe the execution mode of movements at different command frequencies of the stepper motor, the delay time in executing commands for different operating frequencies of the stepper motor, and finally, the displacement on a curve with an "S"-shaped acceleration profile.

The displacement mode of the feed system during the tests is presented below. The movement is carried out in packages of 5 microsteps. One step of 1 µm consists of 5 microsteps of 0.2 µm each, with a pause between them of $T_{\mu p}$ ms. The command sequence is shown in **Table 9.1**:

Table 9.1 Sequence of a step of 1 µm

Microstep	**Micro**	Microstep	**Micro**	Microstep	**Micro**	Microstep	**Micro**	Microstep
0.2 µm	**Pause**	0.2 µm	**Pause**	0.2 µm	**Pause**	0.2 µm	**Pause**	0.2 µm

where: F_{PLC} – commanded frequency from the Programmable Logic Controller - PLC [Hz].

The frequencies used for testing and their corresponding pauses are highlighted in **Table 9.2**:

Table 9.2 Micro pause values based on frequency

F_{PLC} [Hz]	**$T_{\mu p}$ [ms]**
100	10
200	5
500	2
1000	1

Between each execution of a 1 µm step, another pause is given, and the sequence is presented in **Table 9.3**. The pause value is set from the Programmable Logic Controller (PLC), chosen for movements in the shortest possible time and for the motor to start moving again for the next 1 µm step. Thus, the inertia-induced movement of the MPP rotor from the previous execution is avoided.

Table 9.3 Sequence of a successive 1 µm step

Step	**Pause**	Step	**Pause**	Step	…
1 µm		1 µm		1 µm	

Table 9.4 shows the sequence of the feed system movement/displacement.

Table 9.4 Movement sequence

Step of 1 µm									**Pause**	**Step of 1 µm**									⋮
0.2 µm	$T_{\mu p}$	0.2 µm	$T_{\mu p}$	0.2 µm	$T_{\mu p}$	0.2 µm	$T_{\mu p}$	0.2 µm		0.2 µm	$T_{\mu p}$	0.2 µm	$T_{\mu p}$	0.2 µm	$T_{\mu p}$	0.2 µm	$T_{\mu p}$	0.2 µm	

The feed system utilizes two types of movements suitable for the microEDM+US process, namely:

1. Technological – used for short distances and precise positioning during processing;

2. Auxiliary – used for longer distances without precision, for quick retractions or approaches.

In this case, the advancement system utilizes the movement sequence from **Table 9.4**, to execute a motion over a long distance (> 10 µm). The testing is focused on the auxiliary movement type because it is more challenging to achieve.

Within the software, two special commands are implemented [37] [38]:

1. Short-circuit exit (priority 0) – the main objective is to prevent damage to the tool-electrode and the occurrence of an electric arc. Thus, after 0.2 ms, when it is observed that the tool-electrode has entered into a short-circuit, the electroerosion pulses are blocked, and simultaneously, the command for auxiliary displacement (rapid retraction) is initiated. Therefore, during the retraction, no voltage is applied to the tool-electrode, eliminating the risk of an electric arc.

2. Advance of 0.2 µm (priority 1) – 100 discharges are analyzed to determine the decision for an advance or retraction of 0.2 µm.

Ultrasonic oscillation consists of two semiperiods (**Figure 9.5**), with the second semiperiod, during stretching the dielectric liquid (due to capillary phenomena caused by the micrometric size of the work gap in microEDM), considered favorable for discharges. In each semiperiod, the discharge is monitored, including its position, and the moment of its occurrence.

f the discharge with a duration t_i marked in green (see **Figure 9.5** occurs after the beginning of the semiperiod (after 12.5 µs), corresponding to a nominal frequency of 40 kHz, it means it entered the favorable semiperiod.

If the discharge occurs before that, then it is in the unfavorable semiperiod.

The microEDM+US process is guided according to a strategy similar to the one below, with parameter values that can be modified/adjusted experimentally.

Each discharge is counted after a maximum of 100 discharges have occurred. A decision is made based on the majority of discharges. If they are in the favorable semiperiod, a single impulse, commanded by MPP, is used to advance, with an axial increment of 0.2 µm. If they are in the unfavorable semiperiod, a single impulse is commanded for retraction, with an axial increment of 0.2 µm.

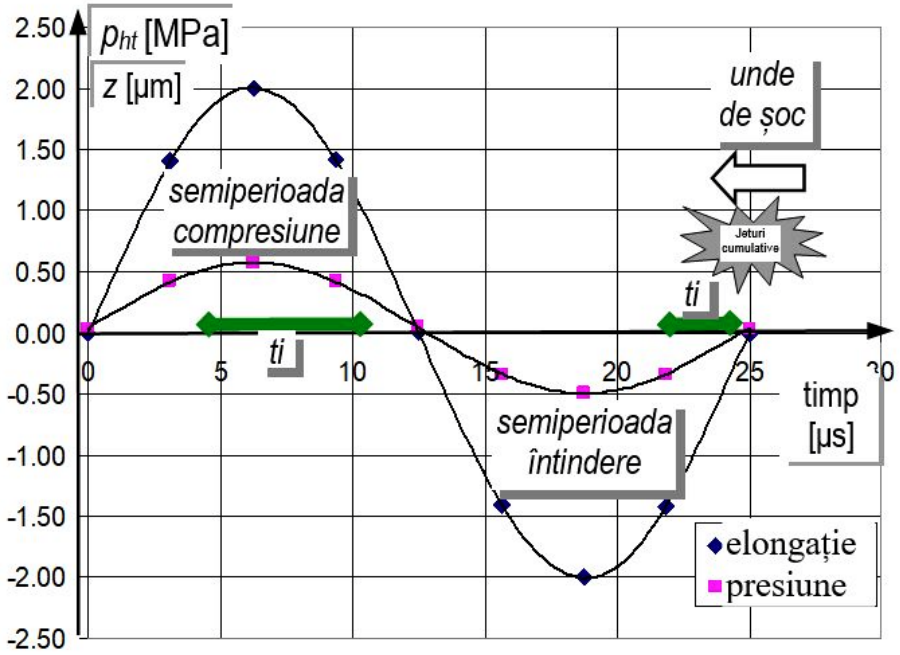

Figure 9.5 The two semiperiods associated with ultrasonically induced cavitation in microEDM+US, according to[16]

9.2.1. Step execution modes test

In the first stage, it will be tested whether the feed system executes all the commanded steps at different frequencies. From the PLC, displacement over a distance of 200 µm has been selected at frequencies of 100, 200, 500, and 1000 Hz in both directions, repeated 2 times. The results are presented in **Table 9.5**:

Table 9.5 Step loss for a movement distance of 200 µm

Nr. crt.	Frequency commanded by PLC [Hz]	SENSE	Electronic travel distance [µm]	Physical travel distance [µm]	Difference [µm]
1	100	DOWN	199	189	-10
2	100	DOWN	199	183	-16
3	100	UP	199	187	-12
4	100	UP	199	207	+8
5	200	DOWN	199	179	-20
6	200	DOWN	199	187	-12
7	200	UP	199	189	-10
8	200	UP	199	204	+5
9	500	DOWN	199	193	-6
10	500	DOWN	199	181	-18
11	500	UP	199	189	-10
12	500	UP	199	205	+6
13	1000	DOWN	199	187	-12
14	1000	DOWN	199	181	-18
15	1000	UP	199	177	-22
16	1000	UP	199	197	-2

The electronic travel distance is highlighted by the PLC. This implies that the pulses sent to the advance system are electronically counted. Theoretically, there are 200 pulses that should be counted, but there is a difference of 1 µm for two reasons:

1. The electronic travel distance is obtained by counting pulses of 0.2 µm and dividing them by 5. The division is done as an integer, with no rounding, so the value after the decimal point is not taken into account.;

2. The microcontroller generating the advance pulses has a scan time of approximately 1 µs, while the PLC displaying the pulses has an independent clock, and the scan time varies between 5 - 10 ms. The communication between the two devices is asynchronous, and the first pulse is always lost.

The physical travel distance is measured through a comparator with a division value of 2 µm (**Figure 9.4**).

The feed system loses steps at every test frequency. Although the values are high (in terms of precision), this type of movement is only used for rapid approach or retraction of the electrode-tool. However, fast movements do not require high precision with the attribute of a low response time to take the system out of critical situations, short-circuit between the tool electrode and workpiece, or continuous arc, respectively, open circuit. Precision movements are commanded step by step, with an increment of 0.2 µm. These are necessary for technological approaches, which directly influences the precision and quality of the processed surface.

9.2.2. Response time test

In the second stage, the response time is tested at different frequencies. The oscillograms that follow were created and provided by EDMing SERV CONSULT SRL.

Returning to the measurement of response time, **Figure 9.6** and **Figure 9.7** are presented:

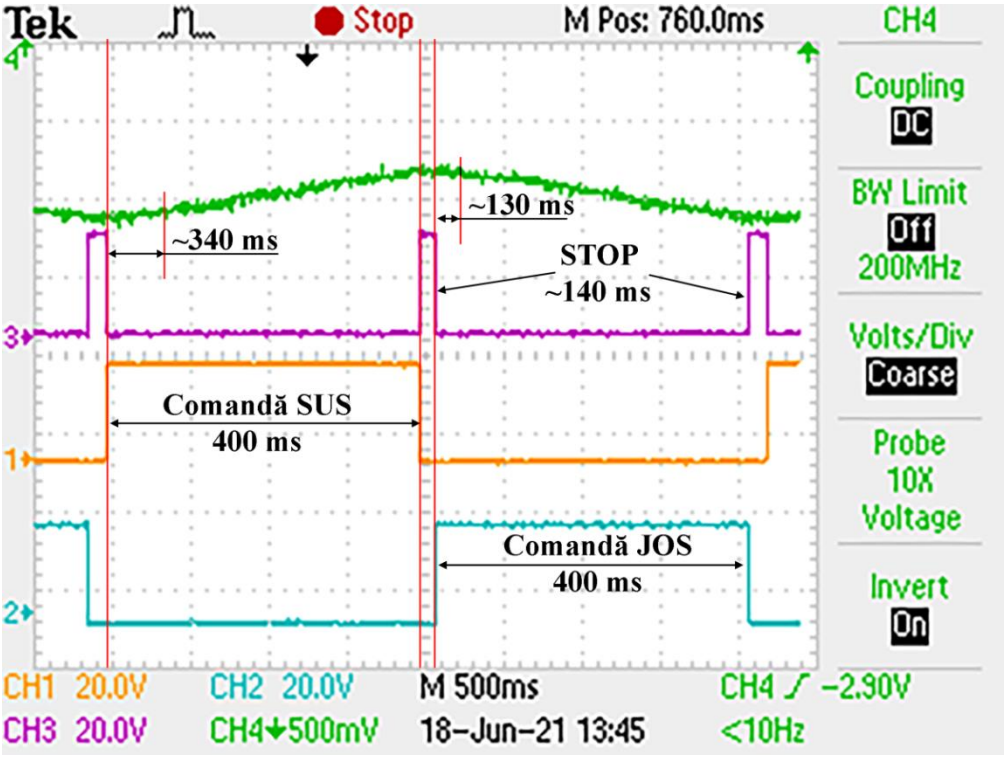

Figure 9.6 Response time at a frequency of 500 Hz with a STOP duration of 140 ms

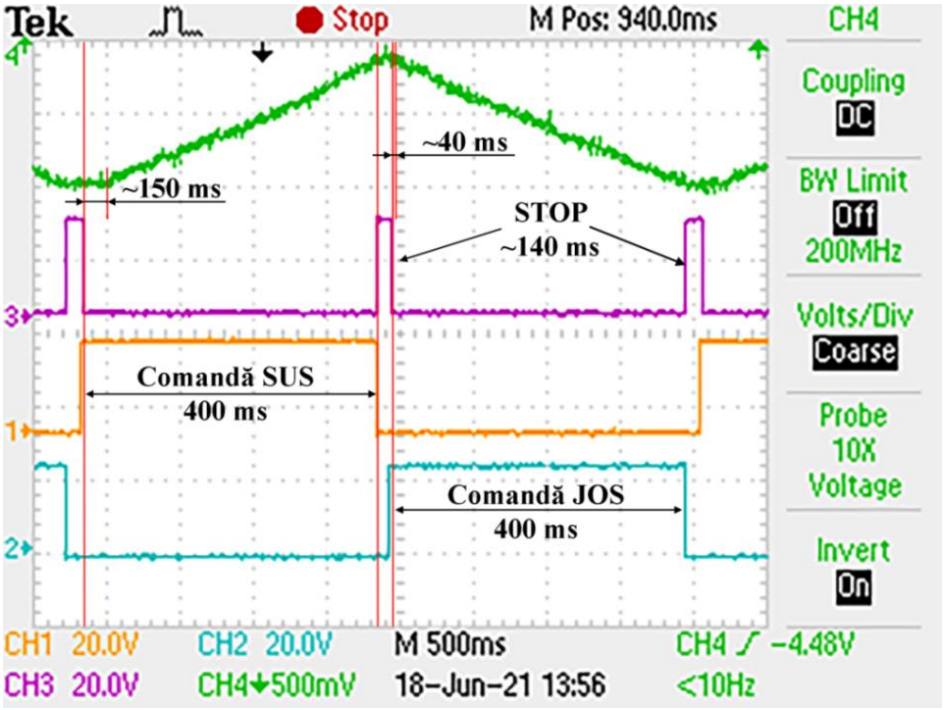

Figure 9.7 Response time at a frequency of 1000 Hz with a STOP duration of 140 ms

In **Figure 9.6**, there is a delay in the rapid ascent command of 340 ms and 130 ms during descent, while in **Figure 9.7**, a delay of 150 ms during ascent and 40 ms during descent is recorded. It is observed that the response time is much better at the starting frequency of 1000 Hz. Therefore, it is recommended to use this frequency as the starting frequency for rapid displacement commands.

9.2.3. S-curve movement test

In the third stage, the goal is to verify if the feed system performs the displacement on an "S"-shaped curve (**Figure 9.8**).

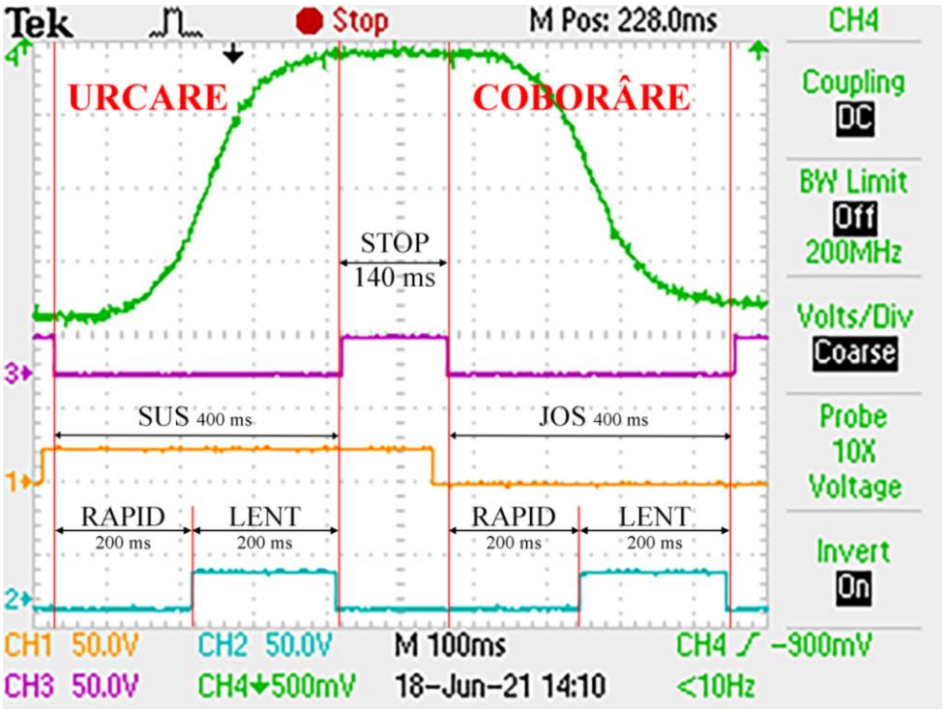

Figure 9.8 Displacement on the "S"-shaped curve at a frequency of 1000 Hz with an UP and DOWN duration of 400 ms

Chapter 10. Final Conclusions, Original Contributions and Research Directions

The conclusions drawn from the research stages and the achievement of the objectives outlined in Chapter 5 are as follows:

The conceptual design of the feed system for ultrasonically assisted microelectroerosion is based on formulating key functions and structuring them by establishing interactions among the elements of the technological system. These elements respond to the requirements of the hybrid ultrasonically assisted micro-electroerosion process and fulfill these demands, as follows:

- Execution of two types of movements: *technological* advances/retractions for the material removal process and *rapid* movements to exit from short-circuit or continuous arc between the electrode-tool surfaces and the workpiece, as well as open circuit;
- Monitoring the position of the electrode-tool relative to the machined surface, meeting the precision requirements imposed by electroerosive micromachining;
- Execution of movements with minimal response time under the conditions of carrying out the process in an extremely narrow work gap, 0 - 5 μm, which varies due to the ultrasonic vibrations of the electrode-tool;
- Execution of movements with a velocity and acceleration profile compatible with the precision required in microelectroerosion; this has implications both on positioning and on the wear of the components of the feed system;
- Perpendicularity of the axis of the feed system to the machine table for meeting the precision conditions prescribed for surfaces generated by microelectroerosion;
- Adjustment of the tilt of the axis of the feed system to obtain inclined holes, contributing to the diversification of technological possibilities of the technological system where the feed system is implemented;
- Minimizing the transmission of ultrasonic vibrations from the ultrasonic chain within the feed system by fixing the ultrasonic chain in a horizontal plane that contains the nodal point, with zero amplitude;
- Operating the feed system outside resonance, involving overlaying the eigenfrequency of the feed system over that of external disturbances, especially the operation of the drive motor for the screw-nut mechanism;
- Moving the tool-electrode with a submicronic linear increment, a condition that is compatible with the size of the machining gap in the range of 0 - 5 μm and its variation with the oscillation amplitude of the tool-electrode at ultrasonic frequency.

Technical solutions were established for implementing these functions, equivalent to phase 2 of technological maturity (Technology Readiness Level - TRL2), namely the conceptualization of the feed system for ultrasonically assisted micro-electroerosion.

Two well-established, complementary, and efficient methods were applied, aiming to enhance the product quality of the ultrasonically assisted micro-electroerosion feed system. These methods are the Quality Function Deployment (QFD), focusing on obtaining technical characteristics based on customer requirements prioritized accordingly, and the Failure Mode and Effects Analysis (FMEA), aiming at preventing operational risks from the conceptual phase (TRL 2) and adopting preventive actions leading to economic efficiency.

The technical solutions resulting from the application of the two quality improvement methods were implemented in the detailed design phase of the product, the ultrasonically assisted micro-electroerosion advance system, resulting in the following configuration:

- Five-phase stepper motor to achieve small native angular steps, actuated by a digital driver controlling micropositioning. In correlation with the lead of the screw-nut mechanism with rollers, it ensures a linear increment of 0.2 μm;
- Elastic coupling, which compensates for potential non-coaxialities between the motor axis and the screw axis with rollers, while transmitting the rotational torque with a delay compatible with the requirements of the microelectroerosion process with ultrasonic electrode-tool vibration;
- Screw-nut mechanism containing three rollers arranged around the lead screw at angles, ensuring superior roller-screw contact through a lever system that increases the closing force of the nut containing the rollers, contributing to increased positioning accuracy;
- Fixed bearing at one end of the roller screw with an angular contact ball bearing with two rows of balls and free bearing at the opposite end, through a guide column with a linear bearing (grooved ball bushing); the column, solidary with the nut, is constrained to perform only a vertical translation movement, having a flat surface in contact with a guide roller, whose relative position to the column is adjusted using an eccentric axis on which the roller is mounted;
- Ultrasonic chain clamping system using prisms that make contact with the ultrasonic chain in the nodal plane area of the concentrator, determining the elongation size so that the ultrasonic vibrations transmitted into the feed system do not affect the precision and quality of the processed surface;
- The ultrasonic chain containing a concentrator, cylindrical-conical, which has at its end the electrode-tool for micromachining, positioned in a ventral region, the point of maximum amplitude;

Modeling and simulating the operation of the feed system for ultrasonic assisted microelectroerosion revealed the following:

- The deformations of the lead screw have lower values compared to the linear positioning increment of the feed system of 0.2 μm for various operating positions and do not affect the processing accuracy;
- The feed system operates outside resonance because its eigenfrequency does not overlap with the driving frequency of the stepper motor;
- The ultrasonic chain operates under resonance conditions, with the transducer frequency equal to that of the concentrator, which includes the tool-electrode.

The technological process for designing the advance system for ultrasonically assisted microelectroerosion was conceived, followed by the execution of the product and testing under laboratory conditions – achieving Technology Readiness Level 4 (TRL 4). Thus, the resonance operation of the ultrasonic chain, incorporating the tool, was achieved, *a prerequisite for ultrasonically assisted microelectroerosion*. The advance system performs rapid movements to eliminate short-circuits or continuous arcs between the surfaces of the electrode-tool and the workpiece, as well as the idle state (lack of electroerosive discharges), ensuring the stability of the micromachining process. The response time to rapid movements, recommended to be performed at a specific stepping motor drive frequency, is compensated by a control strategy implemented on the programmable logic controller, preventing the degradation of the process. The movement is

confirmed to follow an "S" velocity profile, preventing shocks during operation and contributing to achieving the required positioning precision in ultrasonically assisted microelectroerosion..

By completing the established research stages, contributions have been made to the doctoral thesis topic, *research on enhancing performance of feed systems for ultrasonic asssisted microelectroerosion,* involving both theoretical and applicable contributions:

Theoretical contributions

- Phenomenological characterization of ultrasonically induced cavitation in the machining interstice and its influence on the material removal mechanism in ultrasonically assisted microelectroerosion;
- Characterization of the behavior of the feed system under ultrasonic assistance in microelectroerosion;
- Phenomenological characterization of the resonance entry of the feed system by overlaying the eigenfrequency of the feed system with the frequency of the stepper motor control system;
- Development of the operating methodology for the feed system in microEDM+US outside resonance - avoiding the overlap of its eigenfrequencies with the drive frequencies of the stepper motor at different operating regimes;
- Development of the methodology for achieving the resonance condition of the ultrasonic chain, which integrates the tool-electrode for ultrasonic assisted microdrilling;
- Development of the simulation methodology for the deformations of the lead screw for various operating positions of the rollers within the displacement and positioning mechanism of the advance system.

Applicable contributions

- Conceptual design of an efficient feed system for ultrasonic assisted microelectroerosion at Technology Readiness Level 2, TRL2;
- Efficient application of established and complementary quality improvement methods that led to solutions for enhancing the performance of the feed system for ultrasonic assisted microelectroerosion;
- Augmenting the FMEA method with an additional stage focusing on prioritizing actions taken to prevent product dysfunctions based on the economic efficiency number, determined by the product of implementation speed, implementation cost, and the impact on reducing the risk associated with dysfunction;
- Detailed design of an efficient feed system for ultrasonic assisted microelectroerosion, enabling its physical realization and functionality to enhance technological performance under *reduced implementation costs*;
- Detailed design of the ultrasonic chain, integrating the electrode-tool for ultrasonic assisted microelectroerosion, as well as the subassembly for its attachment to the feed system to ensure resonance conditions and prevent the transmission of ultrasonic vibrations within the technological system – the working head of the microEDM machine – that could affect processing precision;
- Modeling and simulation of the operation of the feed system for ultrasonic assisted microelectroerosion, analyzing its eigenfrequency and deformations under relevant operating conditions. Ensured avoidance of resonance with the stepping motor drive frequency and verified deformations that would not compromise processing precision under relevant operating conditions;

- Modeling and simulation of the operation of an ultrasonic concentrator, integrating the electrode-tool for ultrasonic assisted microelectroerosion, and achieving the necessary resonance condition for the operation of the ultrasonic chain;
- Designing the technological process for producing a feed system, enabling improved technological performance, including precision, quality of the processed surface, productivity, and relative volumetric wear;
- Designing the technological process for producing an ultrasonic chain that integrates the electrode-tool for ultrasonically assisted microelectroerosion and the clamping subassembly on the feed system, executing them in resonance conditions with the ultrasonic generator and without transmitting ultrasonic vibrations to the clamping device and, implicitly, to the microEDM+US technological system, affecting the precision of processing;
- Implementing and testing a feed system for ultrasonically assisted microelectroerosion in laboratory conditions – Technology Readiness Level 4 (TRL 4), which confirmed the viability of the adopted design solutions.

Future research directions

After achieving the objectives outlined in the doctoral thesis, the following research directions are opened to enhance the technological performance of ultrasonically assisted microelectroerosion:

- Experiments on the feed system under conditions close to real operation (TRL 5 and 6) to validate the models and simulations that led to the development of the advancement system for microEDM+US, tested in laboratory conditions (TRL 4);
- In-depth investigation of deformations between the lead screw and rollers based on Contact Mechanics theory, using Finite Element Method and Boundary Element Method;
- Design and implementation of other high-performance types of feed systems suitable for ultrasonically assisted microelectroerosion, with new configurations, arrangement of components, and types of roller or ball drive;
- Developing feed systems in other types of loops: closed and hybrid, allowing for increased positioning precision, reduced response time, displacement increment, and system vibrations;
- Explore the use of different materials for the components of feed systems, aiming to simplify their structure and reduce the response time for retraction and advancement commands.

Selective Bibliography

[1] Ghiculescu, L.D., Curs Tehnologii Neconvenționale, Faculatea de Inginerie Industrială și Robotică, Universitatea Națională de Știință și Tehnologie Politehnica București, disponibil la: https://curs.upb.ro/2023/course/view.php?id=4864 , accesat la: 08.07.2023;

[2] Chatti, S., Laperriere, L., Reinhart, G., Tolio, T., CIRP Encyclopedia of Production Engineering, Springer (2019), ISBN: 978-3-662-53120-4;

[3] Ghiculescu L.D., Schulze H. P., Marinescu N., Comparison between gas bubble life duration at classic and ultrasonic aided EDM finishing, Academic Journal of Manufacturing Engineering, 7 (2009) 63-68;

[4] Schulze H.-P., Wollenberg G., Herms R., Mecke K., Gas bubble morphology in small working gaps at spark erosion, Annual report Conference on Electrical Insulation and Dielectric Phenomena, 17 (2004) 534 – 537, DOI: 10.1109/CEIDP.2004.1364305 ;

[5] Ghiculescu, L.D., Marinescu, N. I., Jitianu, G., Seritan, G., On precision improvement by ultrasonics-aided electrodischarge machining, Estonian Journal of Engineering, pp. 2 – 9, 2009;

[6] Snoeys, R., Dauw, D. F., Kruth, J. P., Survey of Adaptive Control in Electro Discharge Machining, Journal of Manufacturing Systems, 2 (1983) 147-164, DOI: 10.1016/S0278-6125(83)80028-4;

[7] Ghiculescu, L.D., Prelucrări neconvenționale, ISBN: 973-652-975-4, București, 2004;

[8] Jahan M. P., Micro-Electrical Discharge Machining, Chapter 4 in *Nontraditional Machining Processes*, J. Paulo Davim, editor, Springer (2013), ISBN: 978-1-4471-5179-1;

[9] Schubert, A., Zeidler, H., Hackert-Oschätzchen, M., Schneider, J., & Hahn, M., Enhancing Micro-EDM using Ultrasonic Vibration and Approaches for Machining of Nonconducting Ceramic, Journal of Mechanical Engineering, 59 (2013) 157-158, DOI: 10.5545/sv-jme.2012.442 ;

[10] Liu, Q., Zhang, Q., Zhang, M., & Zhang, J., Review of size effects in micro electrical discharge machining, Precision Engineering, 44 (2016) 30-31, DOI: 10.1016/j.precisioneng.2016.01.006 ;

[11] Wong, Y. S., Rahman, M., Lim, H. S., Han, H., Ravi, N., Investigation of micro-EDM material removal characteristics using single RC-pulse discharges, Journal of Materials Processing Technologies, 140 (2003) 303-307, DOI: 10.1016/S0924-0136(03)00771-4 ;

[12] Ghiculescu, L. D., Marinescu, N. I., Nanu, S., Ghiculescu, D., Kakarelidis, G., Finite element method study on machined shape influence at ultrasonic aided and not aided microelectrodischarge machining, Nonconventional Technologies Review, 3 (2011) 33-37;

[13] Marinescu, N. I., Ghiculescu, L. D., Nanu, S., Ghiculescu, D., Kakarelidis, G., Technological parameters comparatively studied by FEM at classic and ultrasonic aided microelectrodischarge machining, Nonconventional Technologies Review, 3 (2011) 51-56;

[14] Ghiculescu, L. D., Contribuții privind finisarea prin procedee neconvenționale a suprafețelor active ale matrițelor, Teză de doctorat, Ingineria și managementul sistemelor tehnologice, 1999;

[15] Ghiculescu, L. D., Inginerie și fabricare asistată de calculator în domeniul prelucrărilor neconvenționale. Îndrumar de laborator, Editura Printech, ISBN 978-606-521-7, 2013;

[16] Ghiculescu, L. D., Marinescu, N. I., Alupei, O., On Overlapping the Pulses on Cumulative Microjets Stage at Ultrasonically Aided Electrical Discharge Machining, Applied Mechanics and Materials, 834 (2016) 126-131, DOI: 10.4028/www.scientific.net/AMM.834.126 ;

[17] Endo, T., Tsujimoto, T., Mitsui, K. Study of vibration-assisted micro-EDM – The effect of vibration on machining time and stability of discharge, Precision Engineering, 32 (2008) 269 – 277, DOI: 10.1016/j.precisioneng.2007.09.003 ;

[18] Jameson, E. C., Electrical Discharge Machining, Machining Technology Association/SME (2001), ISBN: 0-87263-521-X;

[19] Ştefănescu, I. I., Chiriţă, G., & Milea, F., Transmisii și Asamblări cu Șuruburi, Editura Fundației Universitare (2004), ISBN: 973-627-188-9;

[20] ***, Proiectarea sistemului de transmitere șurub piuliță cu bile, disponibil la: https://mec.tuiasi.ro/ro/images/OMM/Cap_4_Proiectarea_TSPB_tabele_dimens_rezemare_2015.pdf , accesat la: 12.03.2020;

[21] ***, Motor pas cu pas CRK564PMBP, disponibil la: http://www.giden.ru/data/PDF/stepping_motors/Oriental_motor/crk-catalogue-e.pdf, accesat la: 12.03.2020;

[22] Ghiculescu, L.D., Calitatea proceselor si produselor, Editura Printech, București, ISBN 978-606-23-0678-6, 2016;

[23] Mikulak, R. J., McDermott, R., & Beauregard, M., The basics of FMEA, CRC Press (2009), ISBN: 978-1-56327-377-3;

[24] Deopale, C. C., Ghiculescu, L. D., Cristea, B. I., Risk Management in the cement industry-improving the risk assessment outcomes by developing of a new methodology for prioritizing the treatment options, Acta Technica Napocensis-Series: Applied Mathematics, Mechanics, and Engineering, 65, 2023;

[25] ***, SKF Roller screws, disponibil la: https://idoc.pub/documents/skf-14489-en-roller-screw-catalogue pdf-wl1px22k9vlj, accesat la: 12.03.2020;

[26] ***, Linear ball bearing, open version, disponibil la: https://www.skfbearingselect.com/ , accesat la: 12.03.2020;

[27] ***, Double row angular contact ball bearing, disponibil la: https://www.skf.com/group/products/rolling-bearings/ball-bearings/angular-contact-ball-bearings/double-row-angular-contact-ball-bearings/productid-3202%20A-2RS1TN9%2FMT33 , accesat la: 12.03.2020;

[28] ***, Linear ball bearing, open version, disponibil la: https://www.minitec.de/en/products/linearfuehrung/linear-bearings/serie-lme/ball-bushing-lme-20-uu , accesat la: 12.03.2020;

[29] Popescu I., Marinescu A., Tonoiu S., Purcărea M., Scule aşchietoare, Dispozitive de prindere a sculelor, dispozitive de prindere a semifabricatelor verificatoare, elemente de proiectare, Editura MATRIX ROM (2002), ISBN: 973-685-741-7;

[30] Cristea, B. I., Ghiculescu, L. D., Deopale, C. C., Eigenfrequency simulation for a roller screw used at feed system for ultrasonically aided micro-electrical discharge machining, IOP Conference Series: Materials Science and Engineering, vol. 1235, 2022;

[31] Cristea, B. I., Ghiculescu, L. D., Deopale, C. C., Modeling and simulation of deformations in the feed system for ultrasonically aided micro-edm, Nonconventional Technologies Review, 25(3), 2021;

[32] Radeș, M., Vibrații mecanice, Printech (2008), disponibil la: http://www.rm.upb.ro/wp-content/uploads/2019/01/Rades/05%20M%20Rades%20-%20Vibratii%20mecanice%201.pdf , accesat la: 12.03.2020 ;

[33] Ghiculescu, L. D., Ultrasonically Aided EDM in *Electrical Discharge Machining (EDM)*, Jahan, M. P., editor, Nova Publisher (2015), ISBN: 1634835913;

[34] *** U.S. DEPARTMENT OF ENERGY, Technology Readiness Assessment Guide, disponibil la: https://www.directives.doe.gov/directives-documents/400-series/0413.3-EGuide-04a , accesat la: 28.06.2021;

[35] *** Technology readiness levels (TRL), disponibil la: https://ec.europa.eu/research/participants/data/ref/h2020/wp/2014_2015/annexes/h2020-wp1415-annex-g-trl_en.pdf , accesat la: 28.06.2021;

[36] *** Definiții TRL, disponibil la: https://uefiscdi.gov.ro/userfiles/file/PNCDI%20III/P2_Cresterea%20competitivitatii%20economiei%20romanesti/TRL.pdf , accesat la: 28.06.2021;

[37] Jitianu, G., EDMing SERV CONSULT SRL, Metodă și echipament pentru maximizarea numărului coincidențelor momentelor amorsării unor descărcări electroerozive într-un mediu dielectric lichid, supus sonocavitației cu un anumit moment prestabilit al fazelor undei ultrasonice asociate, Romania Patent, 2016, disponibil la: https://patents.google.com/patent/RO131031B1/ro?oq=RO+131031 , accesat la: 01.09.2023;

[38] Jitianu, G. EDMing SERV CONSULT SRL - Metodă și echipament pentru corelarea descărcărilor electroerozive cu un semnal generator de sonocavitație, RO131211, disponibil la: https://ro.espacenet.com/publicationDetails/biblio?II=0&ND=3&adjacent=true&locale=ro_RO&FT=D&date=20160630&CC=RO&NR=131211A2&KC=A2 , accesat la 01.09.23;

[39] Cristea B. I., Ghiculescu L. D., Țîțu, A. M., Deopale C. C., Modeling and simulation of an ultrasonic concentrator used in a feed system for ultrasonically aided microedm, Publicat de ACTA Technica Napocensis series-applied mathematics mechanics and engineering Journal, în curs de publicare (2023);

Annex 1 – Published Papers

A. Indexed ISI

A.1 **Cristea B. I.**, Ghiculescu L. D., Țîțu, A. M., Deopale C. C., *Modeling and simulation of an ultrasonic concentrator used in a feed system for ultrasonically aided microedm*, Prezentat la The 22nd International Conference of Nonconventional Technologies (ICNcT) 2023, Publicat de ACTA Technica Napocensis series-applied mathematics mechanics and engineering Journal, awaiting publication (2023);

A.2. Deopale C. C., Ghiculescu L. D., **Cristea B. I.**, *Industry 4.0 in Romania - a practical analysis of the country potential from economic and human resources perspective to support a sustainable development of cement smart factories*, Prezentat la QIEM-ICNcT Conference 2021, Publicat de ACTA Technica Napocensis series-applied mathematics mechanics and engineering Journal, Volumul 64, Numărul 4, 663-674, WOS: 000740057300012 (2022);

A.3. Deopale C. C., Ghiculescu L. D., **Cristea B. I.**, *Risk management in the cement industry - improving the risk assessment outcomes by developing of a new methodology for prioritizing the treatment options*, Prezentat la Innovative Manufacturing Engineering & Energy Conference (IManEE) 2022, Publicat de ACTA Technica Napocensis series-applied mathematics mechanics and engineering Journal, Volumul 65, Numărul 4, 1095-1102, WOS: 000969679100015 (2023).

B. Indexed BDI

B.1. **Cristea B. I.**, Ghiculescu L. D., Deopale C. C., *Modeling and simulation of deformations in the feed system for ultrasonically aided micro-edm*, Nonconventional Technologies Review, Volumul 25, Numărul 3, 54-60, Publicat de **ProQuest**, disponibil la: https://www.proquest.com/docview/2638774059?pq-origsite=gscholar&fromopenview=true&sourcetype=Scholarly%20Journals (2021);

B.2. **Cristea B. I.**, Ghiculescu L. D., Deopale C. C., *Eigenfrequency simulation for a roller screw used at feed system for ultrasonically aided micro-electrical discharge machining*, IOP Conference Series: Materials Science and Engineering, Volumul 1235, Publicat de **ProQuest**, DOI: 10.1088/1757-899X/1235/1/012047 (2022);

B.3. **Cristea B. I.**, Ghiculescu L. D., Dumitru M., *Thermal and Mechanical Influence of Ultrasonically Aided Electrical Discharge Machining on Co-Cr Alloys*, Advanced Materials Research, Volumul 1157, 93 – 107, Publicat de **Scientific.Net**, DOI: 10.4028/www.scientific.net/AMR.1157.93 (2020);

B.4. **Cristea B. I.**, Ghiculescu L. D., *Methods for design Improvement of feed system for ultrasonically aided micro-electrical discharge machining*, 36th IBIMA Conference: 4-5 November 2020, Granada, Spain, ISBN: 978-0-9998551-5-7, disponibil la: https://www.youtube.com/watch?v=0BcRmXfftyk&t, accesat la: 01.01.2024;

B.5. **Cristea B. I.**, Ghiculescu L. D., *Some technological solutions for ultrasonic aiding of micro-electrical discharge machining*, Revista de Tehnologii Neconvenționale, Volumul 23, Numărul 4, 88 – 94, Publicat de **ProQuest**, disponibil la: https://www.proquest.com/scholarly-journals/some-technological-solutions-ultrasonic-aiding/docview/2362896050/se-2, (2019);